Effect of Helical Kink in Antimicrobial Peptides on Membrane Pore Formation

Alžběta Türková[1,2,†‡], Ivo Kabelka[1,2†], Tereza Králová[1], Lukáš Sukeník[1,4], Šárka Pokorná[5], Martin Hof[5], Robert Vácha[1,2,4]

***For correspondence:** robert.vacha@mail.muni.cz (RV)

[†]These authors contributed equally to this work

Present address: [‡]Current address: University of Vienna, Department of Pharmaceutical Chemistry, Althanstraße 14, A-1090 Vienna, Austria

[1]CEITEC – Central European Institute of Technology, Masaryk University, Kamenice 753/5, 625 00 Brno, Czech Republic; [2]National Centre for Biomolecular Research, Faculty of Science, Masaryk University, Kamenice 5, 625 00 Brno, Czech Republic; [4]Department of Condensed Matter Physics, Faculty of Science, Masaryk University, Kotlářská 2, 611 37 Brno, Czech Republic; [5]Department of Biophysical Chemistry, J. Heyrovský Institute of Physical Chemistry of the Academy of Sciences of the Czech Republic, v.v.i., Dolejškova 3, 182 23 Prague, Czech Republic

Abstract Antimicrobial peptides (AMPs) can kill pathogens via the formation of permeable membrane pores. However, matching peptide properties with their ability to form pores remains elusive. In particular, the proline/glycine kink in helical AMPs was reported to both increase and decrease antimicrobial activity. We used computer simulations and fluorescence leakage experiments to show that a kink in helices affects the formation of membrane pores by stabilizing toroidal pores but disrupting barrel-stave pores. The precise position of the proline/glycine kink in the sequence further controls the formation of specific toroidal pore structure: U- or hourglass-shaped. Moreover, we demonstrate that two helical peptides can form a stable kink-like connection with similar behavior as one long helical peptide with kink. The provided molecular-level insight can be utilized for rational design or modification of antibacterial peptides or toxins to alter their ability to form membrane pores.

Introduction

Antimicrobial peptides (AMPs) are ubiquitous components of the innate defense system of many organisms. (1; 2) These peptides can selectively kill bacteria, viruses, fungi, or cancer cells at low concentrations. (3; 4; 5) Despite the discovery of thousands of AMPs, the molecular mechanism of their activity remains poorly understood. One of the most prominent mechanisms of action of AMPs is the formation of membrane pores. There are two well-established pore structures: barrel-stave and toroidal. In the barrel-stave pore structure, all peptides are tightly bound into a bundle with only little effect on neighboring lipids. (6) In contrast, the presence of lipid head groups inside the pore together with peptides is characteristic for toroidal pores. (7) Currently, there is no known relation between the sequences of AMPs and their pore-forming ability due to the practical difficulties of determining the transient structures of membrane pores.

AMPs possess an amphiphilic character with a sequence composed of both hydrophobic and hydrophilic residues arranged in discrete clusters. (8) Such a distribution is thought to be the key factor for binding to the pathogen's membrane and its disruption, while a common positive net charge is responsible for the increased selectivity towards bacterial cells. (9; 10) AMPs are typically

unstructured in solution and frequently adopt an α-helical conformation upon interaction with the membrane. Their sequence can contain proline or glycine residues, which cause perturbation in the regular α-helical pattern. As a result, a substantial number of the known AMPs has been determined to possess a helix-kink-helix motif. (11) The presence of a helical kink has been shown to be biologically relevant or even responsible for the AMP's activity. (12; 13) However, the effect of the kink on antimicrobial activity has been the subject of controversy over the past few decades. Methodologically diverse studies have produced contradictory results, reporting the helical kink to both enhance (14; 15; 16; 17; 18; 19; 20; 21; 22; 23; 24) and reduce (25; 26; 27) antimicrobial effects.

Here, we used computer simulations supported by fluorescence experiments to explain the role of the helical kink in the formation of structurally-different pores. We calculated the free energy associated with pore formation under various conditions using Monte Carlo (MC) simulations with a highly coarse-grained phenomenological model (28; 29). Molecular dynamics (MD) simulations employing a more detailed Martini model (35) confirmed the obtained results and matched structural features of various peptides (Magainin II (30), LL-37 (31), Buforin II (32), δ-lysin (33), Candidalysin (34), and their mutants) with their effect on pore stability. We found that the presence of a kink disrupts barrel-stave, but stabilizes toroidal pores. Moreover, the position of the proline/glycine kink with respect to the hydrophobic patch on AMP determined the peptide arrangement within the toroidal pore. The pore formation of various mutants was further verified using a fluorescence leakage assay on large unilamellar vesicles (LUVs).

Results and Discussion

Contradictory Effect of α-helical Kink on Barrel-stave Pore and Toroidal Pore Mechanism

Firstly, we investigated the effect of general peptide properties on the formation of a barrel-stave pore (BP) and toroidal pore (TP) using MC simulations with phenomenological models (28) (see Figure 1B, C and Figure 2A, B). We found two conditions for efficient BP formation which are in agreement with previously reported findings: *(1)* Strong peptide-peptide interaction, which stabilizes the bundle assembly. (36) In our model, the interaction between the peptides was mediated mainly via hydrophobic interactions, thus the peptide hydrophobic content had to be higher than 50% (patch of $180°$) to interact with both lipid tails and surrounding peptides effectively. *(2)* The peptide should be oriented roughly perpendicular to the membrane plane. Therefore, the overall length of the hydrophobic part should span the membrane thickness and peptide termini have to be composed of either hydrophilic or charged residues. (37) The formation of TPs was observed over a broader range of peptide properties than for the peptides forming BPs. Mainly the hydrophobic content/patch was less than or equal to 50% (patch of $180°$). The complete set of tested parameters and formed pores is provided in Table S1 and Table S2.

Secondly, the role of kink flexibility was investigated by using two models of α-helical peptides:*(1)* Peptides without and *(2)* peptides with a fully flexible kink in the middle. Free energy profiles show that the formation of a BP by peptides without the kink is more energetically favorable, compared to formation of pores by the same peptides with the fully flexible kink (difference up to ~10 kT, Figure 1D). However, the effect of the kink is opposite in peptides forming TP, where fully flexible peptides have lower free energy than the peptides without the kink (difference of up to ~10 kT, Figure 2C). The peptide ability to adapt to the different geometry of BP and TP structures could explain these observations. The tightly-packed bundle of peptides in BP structures assumes a cylindrical shape (Figure 1A), whose packing becomes disrupted by the kink. TPs are more unstructured and peptides with the kink more easily conform to the curved shape of the pore catenoid.

Results from the phenomenological model were verified using the Martini model (35), by which the sequences of a few selected AMPs and their mutants were studied. To investigate the effect of the kink, two types of secondary structures were imposed on peptides: *(1)* fully helical and *(2)*

helical with a kink (for details, see the Methods section). In both cases, wild-type (WT) sequences as well as single-point mutations of kink-forming residues were considered.

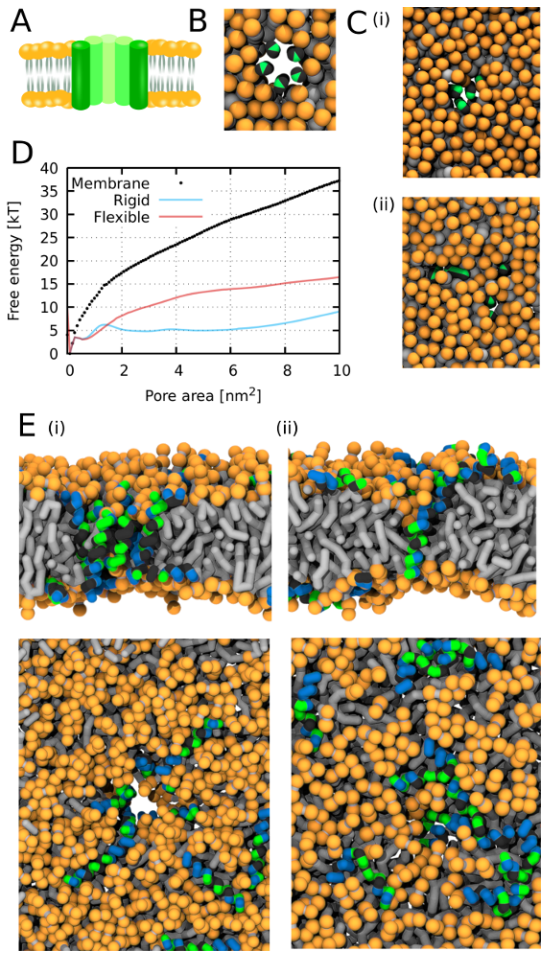

Figure 1. Flexible kink hinders formation of BPs. (A) Schematic representation of BP model. (B) Simulation snapshot of initial BP structure *(top view)* with our phenomenological (O-PSC-NE) model. (C) Stability of BP using peptides with (i) rigid and (ii) fully flexible kink *(top view)*. (D) Free energy profiles of pore formation at low peptide concentration for peptides with and without flexible kink show that peptides without kink lower free energy for pore formation more than flexible ones (O-PSC-NE, peptide length 5 nm, hydrophobicity 270°). (E) Simulation snapshots from Martini simulations with Buforin II peptides. (i) P11L mutation in Buforin II peptides stabilizes formation of BP. (ii) P11G mutation leads to destabilization of BP structure. Top snapshots depict *cross-section view* of the membrane at the position of the peptide aggregate. The bottom snapshots depict *top view* of simulation systems. Color coding: Hydrophobic residues = black, hydrophilic residues = green, positively charged residues = blue, lipid heads = orange, lipid tails = light gray.

Our simulations showed that Buforin II WT (38), with a proline kink in the middle, and its mutant with a glycine kink, P11G, were not able to stabilize BPs, and the pore closed in ~14 μs. In contrast, Buforin II WT* (* refers to the WT with a fixed helical structure) and its helical mutants P11L and P11A remained in the BP structure for the whole of the simulation (50 μs). Snapshots from the end of simulations are depicted in Figure 1E), profiles of pore stability over time (water content in the pore) are in Figure S5 and Figure S6. A comparable pore stability was observed for systems with all considered lipid compositions (POPC, POPC:POPG (1:1), and POPC:POPS (1:1)), see Figure S5 and Table S3. However, the presence of the negatively charged lipids affected BP morphology, which deviated from its regular structure. The deviation was caused by the electrostatic interaction of positively charged residues on Buforin II peptides (charge +6 under physiological conditions), which oriented negatively charged lipid headgroups towards the membrane core (Figure 5D) and disrupted the ideal structure of the BP. For more details, see phosphate density profiles in Figure S13.

The stabilization of TP by peptides with a kink was validated using LL-37, which disrupts POPC membranes (Figure 2D(i). (39) When a kink-forming glycine at position 14 (40) was kept in a helical conformation (WT*) or the peptide was mutated to the helical G14L variant, the stability of TP was decreased and pore closure was observed at ~10 μs (Figure 2D(ii)). Note, however, that G14L mutant of LL-37 was still able to form transient pores (Figure S9). Similarly, WT Candidalysin peptides were capable of stabilizing small (with the minimum pore thickness of 0.5 nm) pores over the whole simulation run (26 μs). When the proline at position 14 was prevented from disrupting the helical conformation, the preformed pores closed within 5 μs.

The above findings from our Martini simulations are in full agreement with the free energy profiles and generic features predicted by our phenomenological models.

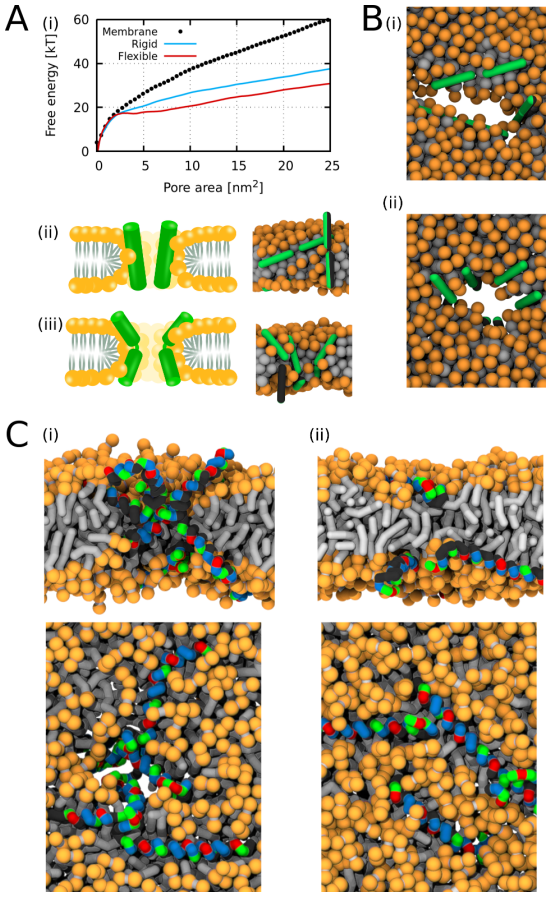

Figure 2. Flexible kink is favorable for formation of TPs. (A) (i) Free energy profiles of pore formation at low peptide concentration for peptides without versus fully flexible kink demonstrate that flexible peptides lower free energy more than those without kink. (PSC AE, peptide length 7nm, half-hydrophobic) Peptides (ii) without and (iii) with fully flexible kink being involved in formation of TP. Schematic representation (left) and simulation snapshots with our phenomenological (PSC-NE) models (right) are depicted. (B) Top view of membrane pores for peptides (i) without and (ii) with fully flexible kink. (C) Simulation snapshots from Martini simulations with LL-37 peptides. (i) WT LL-37 peptides stabilize TP in hourglass shape (ii) G14L mutation in LL-37 peptides leads to destabilization of preformed pores. The top snapshots depict a cross-section view of the membrane at the position of the peptide aggregate, and the bottom snapshots depict the top view of simulation systems. Color coding: Hydrophobic residues = black, hydrophilic residues = green, positively charged residues = blue, negatively charged residues = red, lipid heads = orange, lipid tails = light gray.

The observed effects of the kink on pore stability are in agreement with previous experiments. For example, BP-forming Alamethicin retains its pore-forming function with the rigidifying P14A and G11A, or P14A mutations. (41) An enhanced membrane permeabilization of the P11A and P11L mutants of Buforin II has already been experimentally demonstrated. (19; 38) Moreover, more flexible double mutants P11A/V12P and P11A/V15P of Buforin II had lower membrane permeabilization activity than the P11A and P11L mutants. (42) An enhanced formation of TP by helical peptides with a kink could explain the stronger partitioning of α-helical peptides with an imperfect secondary structure (e.g., a kink in helical AMPs) into the membrane core observed in experiments. (43)

However, when introducing a proline/glycine kink into the peptide sequence, the change in the residue hydrophilicity should also be considered, which together with increased flexibility can alter the peptide adsorption to the membrane. The local concentration of peptides at the membrane could exceed the effect on pore (de)stabilization. Reduced adsorption was demonstrated, e.g., for Melittin mutants (L16G) with increased flexibility. (44) However, after compensating for the adsorption by the addition of negatively charged lipids, the mutant regained its permeabilization ability. (44) Unstructured proline was also suggested to enhance peptide translocation across the membrane (23; 24), but such an effect is beyond the scope of this study.

Different Structures of Toroidal Pores are Influenced by the Kink Position

AMPs with an α-helical kink are capable of driving the formation of structurally diverse TPs. Two TP structures with different orientations of peptides were observed in our simulations (Figure 3A(i),(ii)). The first is called 'U-shaped', inspired by the shape of the peptides, which adopt a bent conformation. The peptide stays on one leaflet with both termini in the headgroup region, and the kink is inserted deeply in the membrane. (45) Candidalysin peptides adopted such a structure in our simulations, see Figure 3B(i). The second TP structure was labeled as 'hourglass'. (46) The peptides span the membrane plane with the kink positioned in the middle. We found such a structure with LL-37 peptides in our simulations, which is in agreement

with experimental findings on LL-37 preferentially forming TPs with a perpendicular orientation. (39) In our phenomenological model, we observed both structures of TP pores. U-shaped pores were observed with peptides with a fully flexible kink, while hourglass pores were found with peptide models with a fixed kink with an inner angle of $135°$ and $90°$. These peptides had hydrophilic end-caps and a length of 5.0 nm.

One of the differences between LL-37 and Candidalysin peptides is the position of the proline/glycine kink with respect to the hydrophobic patch. The Martini model with highlighted proline shows that proline is positioned on the side of the hydrophobic patch in Candidalysin (Figure 3B(i)), while the kink-forming glycine residue in LL-37 peptides is located on the side of the hydrophilic region (Figure 3C(i)). We created mutants that shift the kink residue to the hydrophilic (Candidalysin P14Q/Q15P mutant, Figure 3B(ii)) or hydrophobic (LL-37 I13G/G14I mutant, Figure 3C(ii)) patch by rearranging two adjacent residues. MD simulation of the LL-37 I13G/G14I mutant showed the formation of a U-shaped pore with two peptides adopting such a conformation. The pore was stable for the duration of the simulation ~30 μs, see Figure S7- Figure S9. The Candidalysin P14Q/Q15P mutant switched from a U-shaped TP to an hourglass-shaped TP with perpendicular peptide orientation. The hourglass arrangement of candidalysin peptides appears to be less favorable, as the pore got closed at the beginning of the simulation. Sometimes, small transient pores (with thickness ~ 0.5 nm) appeared throughout the simulation. Therefore, exchanging the positions of two amino acid lead to a change in TP structure from U- to Hourglass-shaped for Candidalysin and from Hourglass- to U-shaped for LL-37, respectively. The position of the kink-forming residue is thus the key that can determine the structure of TPs.

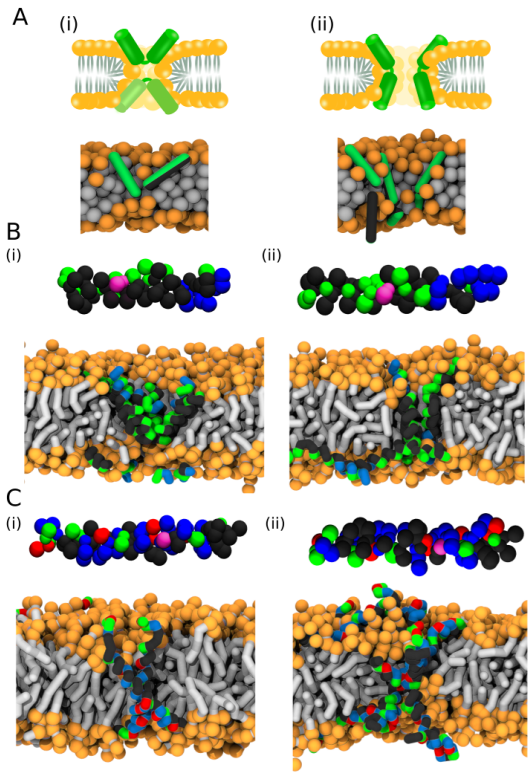

Figure 3. U- and Hourglass-shaped TP structures. (A) Schematic representation *(top)* and simulation snapshots with phenomenological (PSC-NE) models *(bottom)* of (i) U-shaped and (ii) Hourglass TP are depicted. (B) (i) WT Candidalysin peptides adopt U-shaped conformation in membrane core. Peptide model with highlighted proline residue (purple) is depicted. (ii) P14Q/Q15P mutant of Candidalysin (with shifted kink position) induces structural transitions from U- to Hourglass-shaped conformation. Peptide model with highlighted proline residue (purple) is depicted. (C) (i) WT LL-37 preferentially adopts Hourglass-shaped TP structure. Peptide model with highlighted glycine residue (purple) is depicted. (ii) I13G/G14I mutant of LL-37 with kink shifted to hydrophobic patch changes Hourglass-shaped pore structure to U-shaped one. Peptide model with highlighted glycine residue (purple) is depicted. Color coding: Hydrophobic residues = black, hydrophilic residues = green, positively charged residues = blue, negatively charged residues = red, lipid heads = orange, lipid tails = light gray, proline/glycine = purple.

The helix-kink-helix motif is considered to be a motif within one peptide. However, two different helical peptides can interact with each other to form an analogical structure. It has been suggested that a mixture of properly chosen AMPs could possess synergistic interactions responsible for more efficient pore formation. (47) In such a pore, one peptide was found to be inserted in the transmembrane orientation (T-state), whereas the second peptide stayed adsorbed on the membrane surface in parallel orientation (S-state). (47; 51) We observed the synergistic pores with our phe-

nomenological model for long helices with a flexible kink connection (Figure 4A(ii)). Figure 4A(iii) shows the pores formed by peptides with two connected helices, each 3.0 nm in length and with an inner angle of 135° or 90°. The related free energy profiles show the pores formed more easily for peptides with an angle of 135° compared to 90° (Figure 4A(i)).

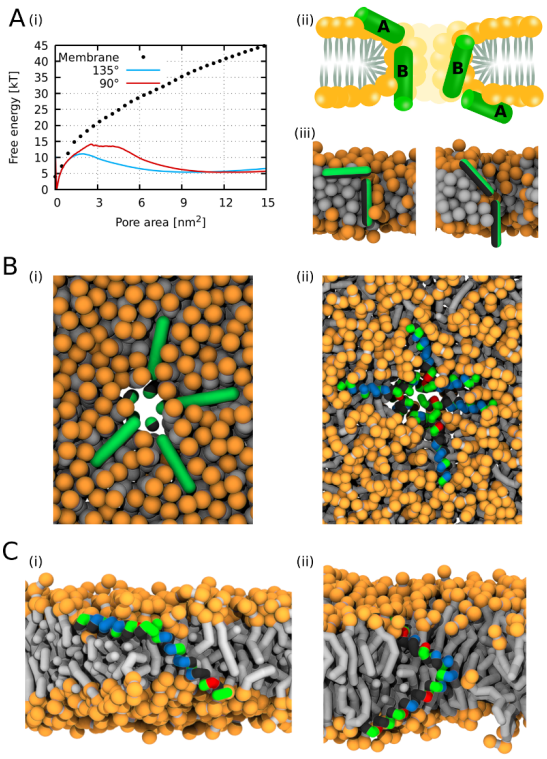

Figure 4. Surface-Transmembrane (ST) pore model. (A) *(i)* Free energy profiles of our phenomenological model with fixed kink (inner angle 135° using PSC-NE model and inner angle 90° using PSC-AE model, peptide length 7.0 nm, half hydrophobic) show that peptides with mutual alignment of 135° are more energetically favorable, *(ii)* Schematic illustration of synergistic pore with end-end interactions between peptides A and B, *(iii)* Simulation snapshot from pore using phenomenological models with alpha = 90° (left) and alpha = 135° (right). (B) *(i)* Phenomenological models and *(ii)* Martini simulations with fully helical Magainin II peptides exhibit analogical ST pore structure. (C) Side view of *(i)* Magainin II peptides shows mutual interactions between their N- and C-termini, whereas *(ii)* δ-lysin peptides exert mutual interactions via their C-termini. Color coding: Hydrophobic residues = black, hydrophilic residues = green, positively charged residues = blue, negatively charged residues = red, lipid heads = orange, lipid tails = light gray.

PGLa and Magainin II are among the best-known AMPs of the Magainin family with synergistic effects. PGLa and Magainin II were found to interact via C-termini with PGLa inside the pore and Magainin II on the membrane surface (49; 47; 50; 51). In agreement with our phenomenological model, the peptides were aligned approximately 135° to each other. Another example of similarly behaving peptides are Magainin II peptides which were reported to form synergistic homomeric pores. (52) Our Martini simulations of Magainin II peptides resulted in pores with peptides interacting via N- C-termini and with an angle between peptides of approximately 135° (Figure 4B(ii), C(i)). Similar behavior was observed for δ-lysin peptides (Figure 4C(ii)). However, δ-lysin peptides interacted via C-termini, and the position of the contact between the peptides was in the middle of the membrane. Such a structure resembles the hourglass TP observed for peptides with the helix-kink-helix motif. The distribution of angles between peptides can be found in Figure S12. The above examples demonstrate the structural similarity of pores formed by peptides with a helix-kink-helix motif and peptides interacting via their termini (for pore stability see Figure S10 and Figure S11). Besides U-shaped and hourglass TP, there is also the structure of Surface-Transmembrane (ST) TP formed by PGLa and Magainin II peptides.

Fluorescent Leakage Assays on Buforin II, LL-37, and their Mutants

Our simulations with both the phenomenological and Martini model revealed that peptide flexibility modulates the formation of BPs and TPs. To further validate our results, Buforin II and LL-37 peptides and their mutants were synthesized and tested using fluorescence leakage assays with LUVs (for details, see the Methods section). For Buforin II peptides, the largest leakage was observed for P11L, followed by a slightly less hydrophobic P11A variant (see Figure 5 A). Significantly lower leakage was found for Buforin II WT with a proline kink, and the lowest leakage was caused by P11G. This is in excellent agreement with the stability of pores in our simulations – Figure 5 C and previous experimental findings. (19; 32) Moreover, LL-37 peptides exhibited greater leakage for the WT than

for the G14L mutant, in agreement with the simulations. Together this confirms that the presence of a flexible kink hinders the formation of BPs but promotes TPs.

Conclusions

We investigated the effect of the proline/glycine kink in helical peptides in membranes using free energy calculations of pore formation with a phenomenological model and pore stability simulations with a more detailed Martini model employing specific peptide sequences. Our multiscale simulation approach supported by fluorescent leakage assays showed that the flexible peptide kink in the helical structure facilitated the formation of toroidal pores (TPs) but caused the instability of barrel pores (BPs).

We found that fully helical Buforin II mutants formed BPs, while the WT and glycine mutants with the kink in the middle did not. The formation of TPs was investigated on LL-37, Candidalysin, δ-lysin, and Magainin II peptides and their mutants. The presence of a proline/glycine kink was demonstrated to stabilize TP. The exact structure (Hourglass or U-shaped) was modulated by the position of the kink in the sequence. Moreover, we showed that a flexible connection between two helices could have the same effect as a kink. In other words, TPs can also be stabilized by helical peptides that strongly interact via termini, effectively forming a helix-kink-helix structure. Such ST pore structures were observed for Magainin II and δ-lysin peptides.

This study provides a comprehensive molecular rationalization of the effect of a proline/glycine kink in helical peptides in the context of membrane pore formation. As most of well-studied AMPs form TPs, a design strategy involving inclusion and correct positioning of a kink-forming residue could yield more potent antimicrobial peptides or less toxic drug-carrying peptides.

Materials and Methods

Computational Simulations

Two conceptually distinct models with a different level of coarse-graining were employed. The first model was a phenomenological model of an α-helix, parametrized as a spherocylinder with a hydrophobic patch. (28) With respect to the hemispherical end-caps, we distinguish two types of phenomenological model - (1) with attractive end-caps (PSC-AE) and (2) with non-attractive end-caps (PSC-NE). To be able to investigate the effect of the kink, we connected two spherocylinders in a peptide by a harmonic bond. The equilibrium length of the harmonic bond was equal to the spherocylinder diameter or zero, leading to PSC or O-PSC models, respectively. The model was developed to be compatible with the three-bead lipid model by Cooke and Deserno, (54) which is an implicit solvent model that captures the membrane elastic properties and phase transition of a lipid bilayer. Peptide parameters (length, hydrophobicity, and flexibility of kink) were systematically varied. The simulations were performed with the Monte Carlo method using the Metropolis algorithm implemented in our freely available code on github.com/robertvacha/SC. We used a prismatic unit cell of about $17 \times 17 \times 30$ nm with periodic boundary conditions. The lipid bilayer was assembled in the XY-plane using 500 lipid molecules and kept at zero tension. After membrane equilibration, peptides were added to the system in a random spatial and orientational distribution. The concentration of peptides and lipids can be expressed as the Peptide-to-Lipid (P/L) ratio. Here, we simulated systems with P/L 1/250, 1/100, 1/50, and 1/25. We used a small peptide concentration to prevent the formation of multiple simultaneous large pores.

Free energy of pore formation was calculated using the Wang-Landau (WL) method. (55) In our simulations, the pore was defined as an area in a membrane plane without lipid tails (bin size of 0.09 nm^2). The area of the largest pore was selected as the reaction coordinate, which was previously shown to be suitable for the free energy calculations of pore formation. (29; 56) The free energy profiles for small pores, with an area less than 2 nm^2 were obtained using the Boltzmann inversion of spontaneous pore distribution. For effective enhanced sampling of the configurational space, we employed multiple walkers, i.e. parallel run of several clients using the same Wang-Landau

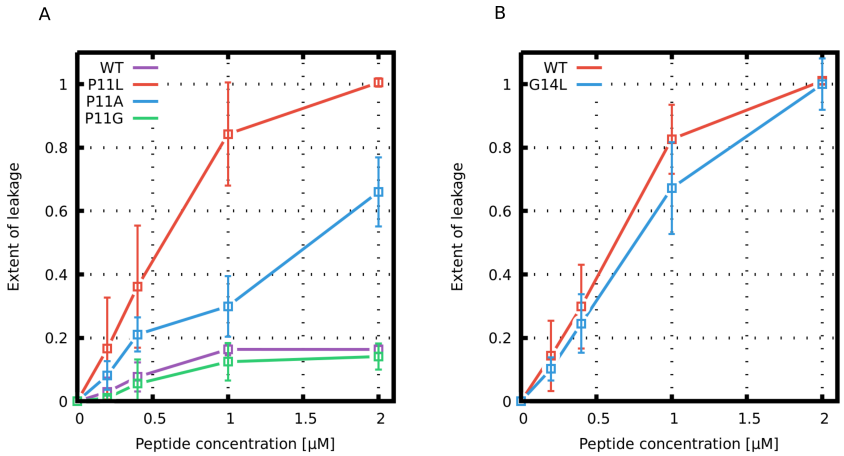

C

System	Mean +- SD
Buforin II WT* in POPC	25 +- 9
Buforin II WT in POPC	10 +- 8
Buforin II P11L in POPC	45 +- 19
Buforin II P11A in POPC	23 +- 8
Buforin II P11G in POPC	17 +- 12
Buforin II P11G* in POPC	49 +- 15
Buforin II P11G^ in POPC	35 +- 12
Buforin II WT* in POPC:POPG (1:1)	7 +- 4
Buforin II WT in POPC:POPG (1:1)	4 +- 3
Buforin II P11L in POPC:POPG (1:1)	16 +- 9
Buforin II P11A in POPC:POPG (1:1)	5 +- 3
Buforin II P11G in POPC:POPG (1:1)	5 +- 4
LL-37 WT in POPC	27 +- 12
LL-37 WT* in POPC	10 +- 6
LL-37 G14L in POPC	15 +- 8
LL-37 I13G/G14I in POPC	25 +-9

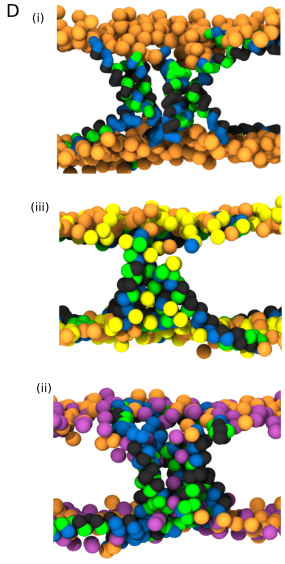

Figure 5. Membrane leakage induced by Buforin II and LL-37 peptides. (A) Fluorescence leakage assays of Buforin II peptides show that P11L mutants are the most effective, followed by helical but less hydrophobic P11A mutant. In contrast, peptides with a kink (higher flexibility), the wild-type and P11G mutant, exibited a lower leakage of fluorescence dye. (B) Fluorescence leakage assays of LL-37 peptides show that G14L mutation slightly hindered membrane leakage, which corresponds to our Martini simulations. (C) Average number of water beads (each corresponding to four water molecules) in pore calculated from Martini simulations of Buforin II and LL-37 peptides. The last 10 μs of simulation was analyzed, and the error is the standard deviation. For details on the models and systems (see Figure S5 and Figure S7). (D) Different lipid composition drives structural transitions from BP to TP structure. Martini snapshots show systems with (i) POPC lipids, (ii) POPC:POPG (1:1) lipids, and (iii) POPC:POPS(1:1) lipids. For the sake of simplicity, only phosphate groups of POPC (orange), POPG (purple), and POPS (yellow) lipids are depicted. Color coding: Hydrophobic residues = black, hydrophilic residues = green, positively charged residues = blue, phosphate groups of POPC lipids = orange, phosphate groups of POPG lipids = purple, phosphate groups of POPS lipids = yellow.

data. Each client started with different initial conditions comprising of randomly selected peptide configuration and membrane with a pre-formed pore of a certain size. The free energy profile was calculated for each of the 156 unique systems, employing several (up to 20) clients. Initial α value was set to 10^{-3}. Calculations of free energy estimate were running unless α value reached a pre-defined value of $\sim 10^{-8}$. In order to increase the precision of sampling, additional simulations with α = 0 were run. No artificial potential was added to the system during the α = 0 simulations, as only histogram was calculated and the free energy profiles were refined accordingly. Again, for the calculation of histogram, up to 10 clients with different initial conditions were employed.

Martini Simulations: The second model was a more detailed Martini coarse-grained model, where roughly four heavy atoms were combined into a single bead. (35) This explicit solvent model is not able to fold proteins, because the secondary structure has to be defined *a priori* and is kept throughout the simulations. We used the helical structure of peptides unless they contained a proline or glycine kink in the sequence. In such cases, we used two secondary structures: (1) α-helical with kink (modelled as a random coil) and (2) fully α-helical for comparison (see Table 1). The membrane was composed of 500 1-palmitoyl-2-oleoyl-sn-glycero-3-phosphocholine (POPC) lipids. For comparison with experiments and to determine the effect of lipid composition, we also investigated lipid mixtures with negatively charged 1-palmitoyl-2-oleoyl-sn-glycero-3-phospho-L-serine (POPS) and 1-palmitoyl-2-oleoyl-sn-glycero-3-phosphoglycerol (POPG) lipids. The mixing ratios were POPC:POPG (1:1) and POPC:POPS (1:1).

The stabilization of the pore by peptides was investigated on preformed pores. First, peptides were placed into a fixed-size pore (maintained by zero box compressibility in the XY-plane). The system was equilibrated in order to obtain the preferred peptide orientation/arrangement. Based on the arrangement, we generated various starting conditions with different peptide arrangements (see Figure S1). The majority of the simulated peptides adopted one particular arrangement in a pore, regardless of the initial configuration used. The only exception was candidalysin peptides with a perpendicular starting configuration, as the peptides were probably unable to reorient into a U-shaped conformation. After additional equilibration, NpT production dynamics at a minimum length of 20 μs were performed. Pore stability was evaluated using water density in the hydrophobic core along the membrane normal. The molecular dynamics simulations with the Martini model (35) were performed using the software package Gromacs 5.0.5.

Molecular Dynamics protocol: The initial configurations of peptides were constructed as α-helical using Modeller 9.11. Peptide configurations were converted to coarse-grained representation by `martinize.py` script, provided by the authors of Martini force field (available at `https://github.com/cgmartini/martinize.py`). For helical proline, backbone angles and dihedrals were set the same as for the other helical residues. Membrane structures were obtained via CHARMM-GUI. (63) Each membrane was composed of 500 lipids, distributed equally in both leaflets. Membrane pore was created by removing lipids in a defined radius from the center of membrane. Afterwards, peptides were placed into a preformed pore. Initial peptide arrangement in a preformed pore is depicted in Figure 6. Steric clashes between peptides and lipids were removed by geometry optimization using steepest descent algorithm. The obtained membrane-peptide configuration was solvated with increased van der Waals radii for both membrane and peptide beads to prevent the water insertion into the membrane hydrophobic core. After solvation, randomly selected water molecules were replaced by NaCl ions of 100 mM concentration. Excess of ions was used to the neutralize system net charge. The complete system was minimized again. Initial particle velocities were generated according to Maxwell distribution corresponding to 323 K. Leap-frog algorithm for integrating Newton's equations of motion was used. System temperature was kept at 323 K using velocity rescaling algorithm (64). Pressure was maintained via Berendesn thermostat at 1.0 bar with time coupling of 5 ps. Semiisotropic coupling scheme was employed. Compressibility was set to 3.10^{-4} bar $^{-1}$ in all directions. Verlet cutoff scheme was employed with radius 1.1 nm. Cutoff for both van der Waals and Coulomb interactions was set to 1.1 nm. Equilibration procedure was performed in five steps with different simulation times: *(1)* 0.5 ns (time step of 2 fs), *(2)* 1.25 ns

Table 1. Overview of peptides used in Martini simulations. H stands for helix, C stands for random coil secondary structure. ∗ points out fully helical secondary structure used for peptides with predicted kink. ∧ symbol points out reduced flexibility of the kink.

Peptide	Label	Sequence & Secondary structure
Buforin 2		seq: TRSSRAGLQFPVGRVHRLLRK
	WT*	ss1: HHHHHHHHHHHHHHHHHHHH
	WT	ss2: HHHHHHHHHHCCHHHHHHHHH
		seq: TRSSRAGLQFLVGRVHRLLRK
	P11L	ss1: HHHHHHHHHHHHHHHHHHHH
		seq: TRSSRAGLQFAVGRVHRLLRK
	P11A	ss1: HHHHHHHHHHHHHHHHHHHH
		seq: TRSSRAGLQFGVGRVHRLLRK
	P11G*	ss1: HHHHHHHHHHHHHHHHHHHH
	P11G	ss2: HHHHHHHHHHCCHHHHHHHHH
	P11G^	ss3: HHHHHHHHHHHCHHHHHHHHH
LL-37		seq: LLGDFFRKSKEKIGKEFKRIVQRIKDFLRNLVPRTES
	WT*	ss1: CCCHHHHHHHHHHHHHHHHHHHHHHHHHHHHHCCCCC
	WT	ss2: CCCHHHHHHHHHHHCHHHHHHHHHHHHHHHHHHCCCCC
		seq: LLGDFFRKSKEKILKEFKRIVQRIKDFLRNLVPRTES
	G14L	ss1: CCCHHHHHHHHHHHHHHHHHHHHHHHHHHHHHCCCCC
		seq: LLGDFFRKSKEKGIKEFKRIVQRIKDFLRNLVPRTES
	I13G/G14I	ss1: CCCHHHHHHHHHHCHHHHHHHHHHHHHHHHHHHCCCCC
Candidalysin		seq: SIIGIIMGILGNIPQVIQIIMSIVKAFKGNKR
	CandKR WT*	ss1: HHHHHHHHHHHHHHHHHHHHHHHHHHHHHHHH
	CandKR WT	ss2: HHHHHHHHHHHHHHCHHHHHHHHHHHHHHHHH
		seq: SIIGIIMGILGNIQPVIQIIMSIVKAFKGNKR
	CandKR P14Q/Q15P	ss1: HHHHHHHHHHHHHHHCHHHHHHHHHHHHHHHH
		seq: SIIGIIMGILGNIPQVIQIIMSIVKAFKGNK
	CandK WT*	ss1: HHHHHHHHHHHHHHHHHHHHHHHHHHHHHHH
	CandK WT	ss2: HHHHHHHHHHHHHHCHHHHHHHHHHHHHHHH
Magainin II		seq: GIGKFLHSAKKFGKAFVGEIMNS
	WT*	ss1: HHHHHHHHHHHHHHHHHHHHHHH
	WT	ss2: HHHHHHHHHHHHCCHHHHHHHHH
		seq: GIGKFLHSAKKFPKAFVGEIMNS
	G13P*	ss1: HHHHHHHHHHHHHHHHHHHHHHH
	G13P	ss2: HHHHHHHHHHHHCCHHHHHHHHH
***δ*-lysin**		seq: MAQDIISTIGDLVKWIIDTVNKFTKK
	WT	ss1: HHHHHHHHCCCHHHHHHHHHHHHHHH
	WT*	ss2: HHHHHHHHHHHHHHHHHHHHHHHHHH

(time step of 5 fs), *(3)* 1 ns (time step of 10 fs), *(4)* 30 ns (time step of 20 fs), *(5)* 15 ns (time step of 20 fs). In step *(1)* - *(4)*, positions of peptide beads were kept restrained with force constant 1000 kJ mol^{-1} nm^{-2}. In step *(5)*, short production dynamics was run, without any positions restraints. We continued the equilibration simulation with production run where only pressure treatment was exchanged to Parrinello-Rahman barostat (65) with coupling time constant 12 ps. All Martini simulations were run with the minimum simulation length of $\sim$ 20 μs.

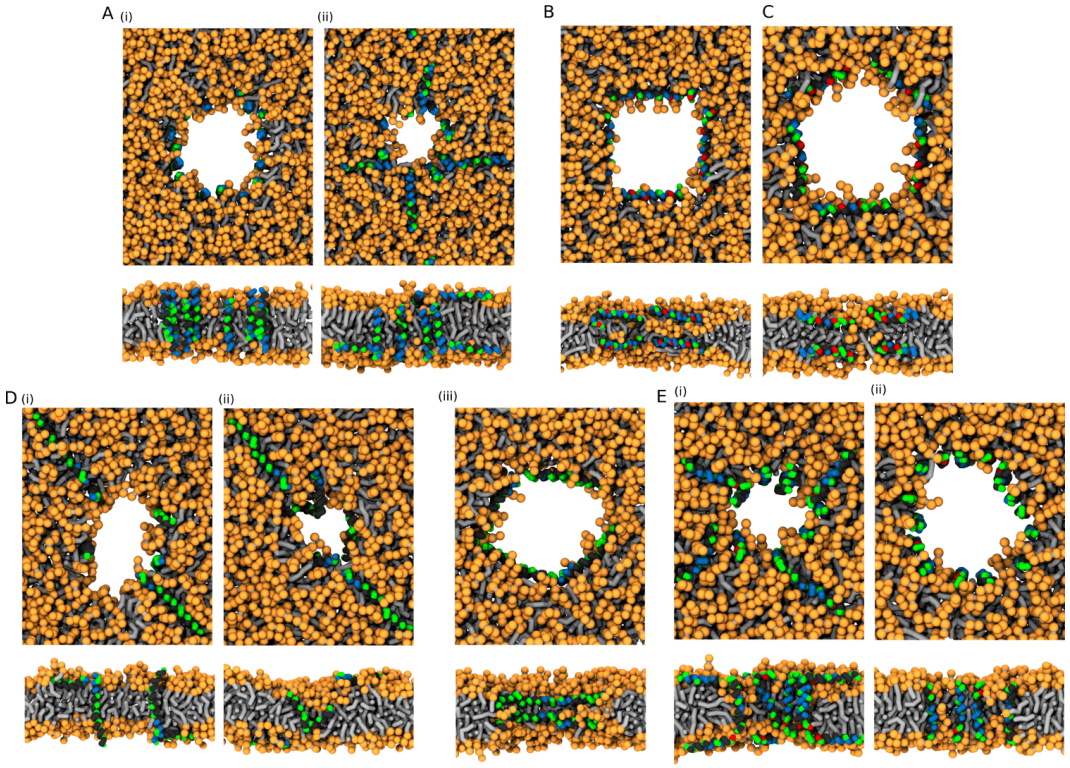

Figure 6. Martini simulations - initial conditions. Based on the preferred peptide orientation within membrane pore, couple of initial configuration were suggested and tested. (A) Buforin II peptides *(i)* 16 peptides oriented perpendicular to membrane plane with antiparallel arrangement in a pre-formed pore, *(ii)* 8 peptides oriented perpendicular to membrane plane with antiparallel arrangement in a pre-formed pore and 8 peptides being placed on membrane leaflets parallel to membrane, (B) 8 LL-37 peptides positioned parallel to membrane plane in pre-formed pore with double-belt pore arrangement, (C) 8 delta-lysin peptides being positioned parallel to membrane in pre-formed pore with double-belt pore arrangement, (D) Candidalysin peptides *(ii)* 4 peptides placed in a pre-formed pore with perpendicular orientation to the membrane plane and 4 peptides on membrane surface oriented parallel to it, *(ii)* 4 peptides in a pre-formed pore in U-shaped conformation and 4 peptides on membrane, *(iii)* 8 peptides in the pore oriented parallel to the membrane plane - double-belt pore arrangement, (E) Magainin II peptides *(I)* 8 peptides in the pore with antiparallel mutual orientation perpendicular to the membrane plane and 8 peptides on membrane with parallel orientation to the membrane plane, and *(ii)* 16 peptides in the pore with antiparallel mutual orientation perpendicular to the membrane plane. Color coding: Hydrophobic residues = black, hydrophilic residues = green, positively charged residues = blue, negatively charged residues = red, lipid heads = orange, lipid tails = light gray.

Experiments

Chemicals: Phospholipids 1-palmitoyl-2-oleoyl-sn-glycero-3-phosphocholine (POPC) and 1-palmitoyl-2-oleoyl-sn-glycero-3-[Phospho-rac-(1-glycerol) Sodium Salt (POPG) were obtained from Avanati Lipids, Inc. (Alabaster, AL, USA). Both phospholipids were dissolved in chloroform; POPC in concentration 25.0 mg/ml (33 mM), POPG in concentration 10.0 mg/ml (13 mM). Lipid solutions were stored at -20°C before use. All peptides were synthetized by JPT Peptide Technologies GmbH (Berlin, Germany). Peptides were dissolved to 1 mM concentration in phosphate-buffered saline (PBS). The buffer composition was 25 mM NaPi (NaH_2PO_4 : Na_2HPO_4 in ratio 3:7), 100 mM NaCl, 1 mM EDTA, the pH was adjusted to physiological value 7.4. Sequence of Buforin II and LL-37 peptides and tested variants is provided in Table Table 2. $NaH_2PO_4.H_2O$, NaOH, NaCl were obtained from Merck (Darmstadt, Germany). Non-ionic surfactant TritonTM X-100 and fluorescent dye Calcein were obtained from Sigma-Aldrich (St.Louis, MO USA). Chelating agent EDTA, Na2HPO4-7H2O, Chloroform Spectronorm, Methanol technical were purchased from VWR (Solon, OH USA). The far-red fluorescent, lipophilic carbocyanine DiIC18(5) oil (DiD) were purchased from Life Technologies Corporation (Eugene, Oregon USA). DiD oil was dissolved in chloroform and stored at -20°C; as 10 mM stock solution and 1 mM working solution.

Table 2. Overview of Buforin II and LL-37 peptides (wild type and mutants) used in the fluorescence experiments.

Buforin II	Sequence
Wild type	TRSSRAGLQFPVGRVHRLLRK
P11L mutation	TRSSRAGLQFLVGRVHRLLRK
P11A mutation	TRSSRAGLQFAVGRVHRLLRK
P11G mutation	TRSSRAGLQFGVGRVHRLLRK

LL-37	Sequence
Wild type	LLGDFFRKSKEKIGKEFKRIVQRIKDFLRNLVPRTES
G14L mutation	LLGDFFRKSKEKILKEFKRIVQRIKDFLRNLVPRTES

Leakage assay: To study the pore formation of Buforin II mutants we employed large unilamellar vesicles (LUV) filled with a self-quenching fluorescence dye, Calcein. After the pore formation the dye leaks out and increase of fluorescence signal can be measured. To measure the same phospholipid concentration in vesicle solution we labeled the lipid membranes with DiD dye which enabled us to determine the lipid concentration fluorescently. After mixing the lipids with the desired ratio POPC:POPG (1:1), we added DiD into the phospholipid mixture at ratio 1:500 (typically 2 nmol of DiD: 1 μmol of phospholipids). Nonpolar solvent (chloroform) was evaporated inside a fume hood. We rotated the glass vial in order to create a thin film over the glass wall. The remaining chloroform was removed by leaving the open vials under vacuum over 2.5 hours. Lipid films were hydrated with 0.5 ml Calcein buffer (self-quenching 35 mM Calcein, 25 mM NaPi, 20 mM NaCl, 1 mM EDTA; pH=7.4) and vortexed vigorously to bring all lipids in suspension. Such solution contains multilamellar lipid vesicles (MLVs). (67) Subsequently, we performed five freeze-thaw cycles at temperatures above the gel-liquid crystalline phase transition (-78.5 ^{o}C/2 min and 30 ^{o}C/0.5 min) (69) Aging of vesicle suspension overnight prior to downsizing by extrusion makes the sizing process easier and improves the homogenity of the size distribution. LUVs were 50 times extruded through 100 nm polycarbonate filter membrane. (68) Unencapsulated Calcein was separated from encapsulated material using HiTrap^{TM} Desalting Columns 5x5ml (matrix is Sephadex G-25 Superfine, cross-linked dextran). Fluorescence spectroscopy was performed with a HORIBA Scientific Jobin Yvon FluoroLog-3 Modular Spectrofluorometer (New Jersey NJ USA) and interfaced to

a computer using FluorEssence™ V3.8. Excitation was set to 495 nm, emission to 520 nm. Excitation and emission slits were 0.25 mm and 1 mm, respectively. Peptides dissolved in a buffer (0.1 mM) were added to obtain the desired Peptide-to-Lipid (P/L) ratio. Finally, 50 μl of nonionic surfactant Triton™ X-100 was added to lyse all remaining LUVs and determine the maximum fluorescence intensity.

Acknowledgement

AT, IK, TK, LS, and RV were supported by the Czech Science Foundation (grant 17-11571S) and the CEITEC 2020 (LQ1601) project with financial contribution made by the Ministry of Education, Youths and Sports of the Czech Republic within special support paid from the National Programme for Sustainability II funds. SP and MH acknowledge support by the Czech Science Foundation (via P208/12/G016). Computational resources were provided by the CESNET LM2015042 and the CERIT Scientific Cloud LM2015085, provided under the programme 'Projects of Large Research, Development, and Innovations Infrastructures'. This work was supported by The Ministry of Education, Youth and Sports from the Large Infrastructures for Research, Experimental Development and Innovations project 'IT4Innovations National Supercomputing Center – LM2015070'.

References

[1] Fosgerau K,Hoffmann T (2015) Peptide therapeutics: current status and future directions. *Drug Discov. Today*, 20(1): 122-128.

[2] Peters B-M, Shirtliff M-E, Jabra-Rizk M-A (2010) Antimicrobial peptides: primeval molecules or future drugs? *PLoS Pathog.*, 6(10): e1001067.

[3] Gaspar D, Veiga A-S, Castanho A-R-B-M (2013) From antimicrobial to anticancer peptides. A review. *Front Microbiol.*, 4: 294.

[4] Falco A, Ortega-Villaizan M, Chico V, Brocal I, Perez L, Coll J-M, Estepa A (2009) Antimicrobial peptides as model molecules for the development of novel antiviral agents in aquaculture. *Mini-Rev Med. Chem.*, 9(10): 1159-1164.

[5] Hoskin D-W, Ayyalusamy R (2008) Studies on anticancer activities of antimicrobial peptides. *Biochim. Biophys. Acta*, 1778(2): 357-375.

[6] Pollard H-B, Arispe N, Rojas E (1995) Ion channel hypothesis for Alzheimer amyloid peptide neurotoxicity. *Cell Mol. Neurobiol.*, 15(5): 513-526.

[7] Sengupta D, Leontiadou H, Mark A-E, Marrink S-J (2008) Toroidal pores formed by antimicrobial peptides show significant disorder. *Biochim. Biophys. Acta*, 1778(10): 2308-2317.

[8] Wimley W-C (2010) Describing the mechanism of antimicrobial peptide action with the interfacial activity model. *ACS Chem. Biol.*, 5(10): 905-917.

[9] Chen Y, Mant C-T, Farmer S-W, Hancock R-E, Vasil M-L, Hodges R-S (2005) Rational design of α-helical antimicrobial peptides with enhanced activities and specificity/therapeutic index. *J. Biol. Chem.*, 280(13): 12316-12329.

[10] Dathe M, Wieprecht T (1999) Structural features of helical antimicrobial peptides: their potential to modulate activity on model membranes and biological cells. *Biochim. Biophys. Acta*, 1462(1): 71-87.

[11] Kozic M, Fox S-J, Thomas J-M, Verma C-S, Rigden D-J (2018) Large scale ab initio modelling of structurally uncharacterized antimicrobial peptides reveals known and novel folds. *Proteins: Struct., Funct., Bioinf.*, 9(9): 736-744.

[12] Vanhoof G, Goossens F-D-M-I-H-D-S, De Meester I, Hendriks D,vScharpe S (1995) Proline motifs in peptides and their biological processing. *FASEB J.*, 9(9): 736-744.

[13] Lee J-K, Gopal R, Park S-C, Ko H-S, Kim Y, Hahm K-S, Park Y (2013). A proline-hinge alters the characteristics of the amphipathic α-helical AMPs. *PloS one*, 8(7), e67597.

[14] Xiao Y, Herrera A-I, Bommineni Y-R, Soulages J-L, Prakash O, Zhang G (2009) The central kink region of fowlicidin-2, an α-helical host defense peptide, is critically involved in bacterial killing and endotoxin neutralization. *J. Innate Immun.*, 1(3): 268-280.

[15] Suh J-Y, Lee Y-T, Park C-B, Lee K-H, Kim S-C, Choi B-S (1999) Structural and functional implications of a proline residue in the antimicrobial peptide gaegurin. *FEBS J.*, 266(2): 665-674.

[16] Lim S-S, Kim Y, Park Y, Kim J-I, Park I-S, Hahm K-S, Shin S-Y (2005) The role of the central l-or d-Pro residue on structure and mode of action of a cell-selective α-helical IsCT-derived antimicrobial peptide. *Biochem. Biophys. Res. Commun.*, 334(4): 1329-1335.

[17] Shin S-Y, Yang S-T, Park E-J, Eom S-H, Song W-K, Kim J-I, Kim Y (2001) Antibacterial, antitumor and hemolytic activities of α-helical antibiotic peptide, P18 and its analogs. *Chem. Bio.l Drug Des.*, 58(6): 504-514.

[18] Suh J-Y, Lee K-H, Chi S-W, Hong S-Y, Choi B-W, Moon H-M, Choi B-S (1996) Unusually stable helical kink in the antimicrobial peptide - derivative of gaegurin. *FEBS Lett.*, 392(3): 309-312.

[19] Kobayashi S, Takeshima K, Park C-B, Kim S-C, Matsuzaki K (2000) Interactions of the novel antimicrobial peptide buforin 2 with lipid bilayers: proline as a translocation promoting factor. *Biochemistry*, 39(29): 8648-8654.

[20] Tieleman D-P, Shrivastava I-H, Ulmschneider M-R, Sansom M-S (2001) Proline-induced hinges in transmembrane helices: possible roles in ion channel gating. *Proteins: Struct., Funct., Bioinf.*, 44(2): 63-72.

[21] Rodriguez A, Villegas E, Montoya-Rosales A, Rivas-Santiago B, Corzo G (2014) Characterization of antibacterial and hemolytic activity of synthetic pandinin 2 variants and their inhibition against Mycobacterium tuberculosis. *PloS one*, 9(7): e101742.

[22] Corzo G, Escoubas P, Villegas E, Barnham K-J, He W, Norton R-S, Nakajima T (2001) Characterization of unique amphipathic antimicrobial peptides from venom of the scorpion Pandinus imperator. *Biochem. J.*, 359(1): 35-45.

[23] Vermeer L-S, Lan Y, Abbate V, Ruh E, Bui T-T, Wilkinson L-J, Kanno T, Jumagulova E, Kozlowska J, Patel J, McLntyre C-A, Yam W-C, Siu G, Atkinson R-A, Lam K-W, Bansal S-S, Drake A-F, Mitchell G-H, Mason A-J (2012) Conformational flexibility determines selectivity and antibacterial, antiplasmodial, and anticancer potency of cationic α-helical peptides. *J. Biol. Chem.*, 287(41), 34120-34133.

[24] Amos S-B-T-A, Vermeer L-S, Ferguson P-M, Kozlowska J, Davy M, Bui T-T, Drake A-F, Lorenz C-L, Mason A-J (2016) Antimicrobial Peptide Potency is Facilitated by Greater Conformational Flexibility when Binding to Gram-negative Bacterial Inner Membranes. *Sci. Rep.*, 6, 37639.

[25] Park S-H, Kim H-E, Kim C-M, Yun H-J, Choi E-C, Lee B-J (2002) Role of proline, cysteine and a disulphide bridge in the structure and activity of the anti-microbial peptide gaegurin 5. *Biochem. J.*, 368(Pt1): 171.

[26] Gehman J-D, Luc F, Hall K, Lee T-H ,Boland M-P, Pukala T-L, Separovic F (2008) Effect of antimicrobial peptides from Australian tree frogs on anionic phospholipid membranes. *Biochemistry*, 47(33):8557-8565.

[27] Liu L, Fang Y, Huang Q, Wu J (2011) A rigidity-enhanced antimicrobial activity: a case for linear cationic α-helical peptide HP (2-0) and its four analogues. *PloS one*, 6(1), e16441.

[28] Vácha R, Frenkel D (2014) Stability of Bicelles: A Simulation Study. *Langmuir*, 30(15): 4229-4235.

[29] Kabelka, I., Vácha, R. (2015). Optimal conditions for opening of membrane pore by amphiphilic peptides. *J. Chem. Phys.*, 143(24), 243115.

[30] Matsuzaki K, Sugishita K, Fujii N, Miyajima K (1995) Molecular basis for membrane selectivity of an antimicrobial peptide, magainin 2. *Biochemistry*, 34(10): 3423-3429.

[31] Turner J, Cho Y, Dinh N-N, Waring A-J, Lehrer R-I (1998) Activities of LL-37, a cathelin-associated antimicrobial peptide of human neutrophils. *Antimicrob. Agents Chemother.*, 42(9): 2206-2214.

[32] Park C-B,Kim H-S ,Kim S-C (1998) Mechanism of action of the antimicrobial peptide buforin II: buforin II kills microorganisms by penetrating the cell membrane and inhibiting cellular functions. *Biochem. Biophys. Res. Commun.* 244(1): 253-257.

[33] Janzon L, Löfdahl S, Arvidson S (1989) Identification and nucleotide sequence of the delta-lysin gene, hld, adjacent to the accessory gene regulator (agr) of Staphylococcus aureus. *Mol. Gen. Genet.*, 219(3): 480-485.

[34] Moyes D-L, Wilson D, Richardson J-P, Mogavero S, Tang S-X, Wernecke J, Murciano C (2016) Candidalysin is a fungal peptide toxin critical for mucosal infection. *Nature*, 532(7597): 64.

[35] Monticelli L, Kandasamy S-K, Periole X, Larson R-G, Tieleman D-P, Marrink S-J (2008) The MARTINI coarse-grained force field: extension to proteins. *J. Chem. Theory Comput.*, 4(5): 819-834.

[36] Gregoria I, Deserno M (2008) Coarse-grained simulation studies of peptide-induced pore formation. *Biophys. J.*, 95(9): 4163-4173.

[37] Vácha R, Frenkel D (2013) Simulations suggest possible novel membrane pore structure. *Langmuir*, 30(5): 1304-1310.

[38] Park C-B, Yi K-S, Matsuzaki K ,Kim M-S, Kim S-C (2000) Structure–activity analysis of buforin II, a histone H2A-derived antimicrobial peptide: the proline hinge is responsible for the cell-penetrating ability of buforin II. *Proc. Natl. Acad. Sci. USA*, 97(15): 8245-8250.

[39] Lee C-C, Sun Y, Qian S, Huang H-W (2011) Transmembrane pores formed by human antimicrobial peptide LL-37. *Biophys. J.*, 100(7): 1688-1696.

[40] Xhindoli D, Pacor S, Benincasa M, Scocchi M, Gennaro R, Tossi A (2016) The human cathelicidin LL-37—A pore-forming antibacterial peptide and host-cell modulator. *Biochim. Biophys. Acta.*, 1858(3): 546-566.

[41] Jacob J, Duclohier H, Cafiso D-S (1999) The role of proline and glycine in determining the backbone flexibility of a channel-forming peptide. *Biophys. J.*, 76(3), 1367-1376.

[42] Xie Y, Fleming E, Chen J-L, Elmore D-E (2011) Effect of proline position on the antimicrobial mechanism of buforin II. *Peptides*, 32(4), 677-682.

[43] Henderson J-M, Waring A-J, Separovi F, Lee K-Y-C (2016) Antimicrobial peptides share a common interaction driven by membrane line tension reduction. *Biophys. J.*, 111(10):2176-2189.

[44] Krauson A-J, Hall O-M, Fuselier T, Starr C-G, Kauffman W-B, Wimley W-C (2015) Conformational fine-tuning of pore-forming peptide potency and selectivity. *J. Am. Chem. Soc.*, 137(51), 16144-16152.

[45] Kolattukudy S-P, Berkowitz P-M-L (2012) Difference between magainin-2 and melittin assemblies in phosphatidylcholine bilayers: results from coarse-grained simulations. *J. Phys. Chem. B*, 116(9): 3021-3030.

[46] Jung J-S, Preston G-M, Smith B-L, Guggino W-B, Agre P (1994) Molecular structure of the water channel through aquaporin CHIP. The hourglass model. *J. Biol. Chem.*, 269(20): 14648-14654.

[47] Salnikov E-S, Bechinger B (2011) Lipid-controlled peptide topology and interactions in bilayers: structural insights into the synergistic enhancement of the antimicrobial activities of PGLa and magainin 2. *Biophys. J.*, 100(6):1473-1480.

[48] Yeh I-C, Olson M-A, Lee M-S, Wallqvist A (2008) Free-energy profiles of membrane insertion of the m2 transmembrane peptide from influenza a virus. *Biophys. J.*, 95(11): 5021-5029.

[49] Westerhoff H-V, Zasloff M, Rosner J L, Hendler R-W, Waal A, Gomes A-V, Juretić D. (1995) Functional Synergism of the Magainins PGLa and Magainin-2 in Escherichia coli, Tumor Cells and Liposomes. *FEBS J.*, 228(2):257-264.

[50] Matsuzaki K, Mitani Y, Akada K-Y, Murase O, Yoneyama S, Zasloff M, Miyajima K (1998) Mechanism of synergism between antimicrobial peptides magainin 2 and PGLa. *Biochemistry*, 37(43):15144-15153.

[51] Strandberg E, Horn D, Reißer S, Zerweck J, Wadhwani P, Ulrich A-S (2016) 2H-NMR and MD simulations reveal membrane-bound conformation of magainin 2 and its synergy with PGLa. *Biophys. J.*, 111(10):2149-2161.

[52] Wakamatsu K, Takeda A, Tachi T, Matsuzaki K (2002) Dimer structure of magainin 2 bound to phospholipid vesicles. *Biopolymers*, 64(6): 314-327

[53] Cheraghi N, Hosseini M, Mohammadinejad S (2018) Pore formation and the key factors in antibacterial activity of aurein 1.2 and LLAA inside lipid bilayers, a molecular dynamics study. *Biochim. Biophys. Acta*, 1860(2):347-356.

[54] Cooke, I. R., Deserno, M. (2005) Solvent-free model for self-assembling fluid bilayer membranes: stabilization of the fluid phase based on broad attractive tail potentials. *J. Chem. Phys.*, 123(22), 224710.

[55] Wang F, Landau D P (2001) Efficient, multiple-range random walk algorithm to calculate the density of states. *Phys. Rev. Lett.*, 86(10), 2050.

[56] Wang Z-J, Frenkel D (2005) Pore nucleation in mechanically stretched bilayer membranes. *J. Chem. Phys.*, 123(15), 154701.

[57] Wimley W C, White S H (1996) Experimentally determined hydrophobicity scale for proteins at membrane interfaces. *Nat. Struct. Mol. Biol.*, 3(10), 842.

[58] Arias M, Prenner E J, Vogel H J (2017) Calorimetry Methods to Study Membrane Interactions and Perturbations Induced by Antimicrobial Host Defense Peptides. *Antimicrobial Peptides*, 119-140.

[59] Mayer L-D, Hope M-J, Cullis P-R, Janoff A-S (1985) Solute distributions and trapping efficiencies observed in freeze-thawed multilamellar vesicles. *Biochim. Biophys. Acta*, 817(1), 193-196.

[60] Nayar R, Hope M-J, Cullis P-R (1989) Generation of large unilamellar vesicles from long-chain saturated phosphatidylcholines by extrusion technique. *Biochim. Biophys. Acta*, 986(2), 200-206.

[61] Braun S, Pokorná Š, Šachl R, Hof M, Heerklotz H, Hoernke M (2017) Biomembrane Permeabilization: Statistics of Individual Leakage Events Harmonize the Interpretation of Vesicle Leakage. *ACS nano*.

[62] Lidman M, Pokorná Š, Dingeldein A P G, Sparrman T, Wallgrend M, Šachl R, Hof M, Gröbner G (2016) The oxidized phospholipid PazePC promotes permeabilization of mitochondrial membranes by Bax. *Biochim. Biophys. Acta*, 858(6),1288-1297.

[63] Jo S, Kim T, Iyer V-G, Im W (2008) CHARMM-GUI: a web-based graphical user interface for CHARMM. *J. Comput. Chem.*, 29(11), 1859-1865.

[64] Bussi, G., Donadio, D., Parrinello, M. (2007). Canonical sampling through velocity rescaling.*J Chem Phys* , 126(1), 014101.

[65] Parrinello M, Rahman A. (1981) Polymorphic transitions in single crystals: A new molecular dynamics method. *J. Appl. Phys.*, 52(12), 7182-7190.

[66] Moyes D-L, Wilson D, Richardson J-P, Mogavero S, Tang S-X, Wernecke J, Murciano C (2016) Candidalysin is a fungal peptide toxin critical for mucosal infection. *Nature*, 532(7597): 64.

[67] Arias M, Prenner E J, Vogel H J (2017) Calorimetry Methods to Study Membrane Interactions and Perturbations Induced by Antimicrobial Host Defense Peptides. *Antimicrobial Peptides*, 119-140.

[68] Mayer L-D, Hope M-J, Cullis P-R, Janoff A-S (1985) Solute distributions and trapping efficiencies observed in freeze-thawed multilamellar vesicles. *Biochim Biophys Acta*, 817(1), 193-196.

[69] Nayar R, Hope M-J, Cullis P-R (1989) Generation of large unilamellar vesicles from long-chain saturated phosphatidylcholines by extrusion technique. *Biochim Biophys Acta*, 986(2), 200-206.

Supplementary Material

Table S1. Combination of parameters for O-PSC-NE model peptides with *fixed* and *flexible* kink. Effect of peptide length (4.0, 5.0, or 7.0 nm), width of hydrophobic patch (150°, 190°, 180°, 230°, 270°, 310°, 350°), on the formation of different pore structures is depicted. TP stands for toroidal pore (without any more closely specified structure, see example in Figure S1), BP for barrel-stave pore, ST for surface-transmembrane pore, X for no binding to the membrane, I/A for peptide insertion to the membrane but no peptide aggregation inside the membrane, S/A for aggregation of peptides in solvent, and DTP for disordered toroidal pore structure, see example in Figure S2.

	flexible	rigid	flexible	rigid	flexible	rigid	flexible	rigid	flexible	rigid	flexible	rigid
patch width [∘]	150		190		230		270		310		350	
length [nm]												
4.0	x	x	x	x	x	x	x	x	x	BP	I/A	I/A
5.0	x	x	x	x	x	x	TP	BP	I/A	BP	I/A	I/A
7.0	TP	S/A	TP	TP	TP	DTP	I/A	DTP	I/A	I/A	I/A	I/A

Table S2. Combination of parameters for PSC-NE and PSC-AE model peptides with *fixed* and *flexible* kink. Effect of peptide length (4.0, 5.0, or 7.0 nm), width of hydrophobic patch (180°), and attractiveness of end-caps (PSC-NE or PSC-AE) on the formation of different pore structures is depicted. TP stands for toroidal pore (without any more closely specified structure, see example in Figure S1), U for U-shaped pore, HG for hourglass pore, BP for barrel-stave pore, ST for surface-transmembrane pore, and DTP for disordered toroidal pore structure, see example in Figure S2.

	PSC-AE with *fixed* kink			PSC-NE with *fixed* kink		
width [°]	length [nm]			length [nm]		
	4.0	5.0	7.0	4.0	5.0	7.0
180	TP	TP	TP	DTP	TP	TP

	PSC-AE with *flexible* kink			PSC-NE with *flexible* kink		
width [°]	length [nm]			length [nm]		
	4.0	5.0	7.0	4.0	5.0	7.0
180	TP	TP	TP/HG	TP	U/HG	U

Table S3. Average number of solvent molecules in the region from ∼ -0.9 to 0.9 nm from membrane center in the last 10 μs. Note that WT$*$ stands for wild-type sequence where kink-forming residue was forced to be α-helical. In case of Buforin II P11G^, only single coil in mutated glycine position has been used as a definition of secondary structure.

System	Mean number	Standard Deviation
POPC	0.7	1.1
LL-37 WT in POPC	27.4	11.9
LL-37 WT* in POPC	9.8	6.1
LL-37 G14L in POPC	15.3	7.8
LL-37 I13G/G14I in POPC	24.6	8.6
Buforin II WT* in POPC	27.6	10.3
Buforin II WT in POPC	10.5	7.6
Buforin II P11L in POPC	43.7	17.8
Buforin II P11A in POPC	23.1	8.6
Buforin II P11G in POPC	7.7	6.0
Buforin II P11G^ in POPC	20.0	14.8
Buforin II P11G* in POPC	21.4	7.4
Buforin II WT* in POPC:POPG (1:1)	6.0	3.6
Buforin II WT in POPC:POPG (1:1)	4.0	3.2
Buforin II P11L in POPC:POPG (1:1)	14.9	8.0
Buforin II P11A in POPC:POPG (1:1)	5.3	3.6
Buforin II P11G in POPC:POPG (1:1)	3.7	3.2
Buforin II WT* in POPC:POPS (1:1)	7.8	4.0
Buforin II WT in POPC:POPS (1:1)	3.8	3.0
Buforin II P11L in POPC:POPS (1:1)	5.4	3.6
Buforin II P11A in POPC:POPS (1:1)	7.7	4.9
Buforin II P11G in POPC:POPS (1:1)	3.9	3.3
Magainin II WT* in POPC	30.1	8.9
Magainin II WT in POPC	16.1	6.8
Magainin II G13P* in POPC	45.3	11.5
Magainin II G13P in POPC	60.3	18.8
δ-lysin WT* in POPC	12.4	5.7
δ-lysin WT in POPC	15.8	6.8
CandK WT* in POPC	6.0	4.3
CandK WT in POPC	6.9	3.4
CandKR WT in POPC	7.1	4.2
CandKR P14Q/Q15P in POPC	6.6	4.5

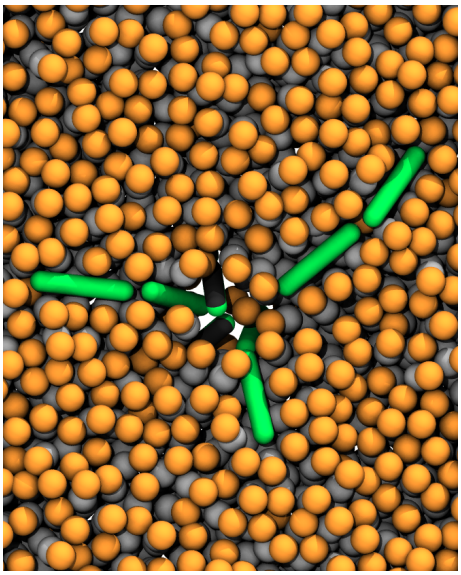

Figure S1. Example of toroidal pore with phenomenological models. Snapshot shows that some peptides (PSC-AE model) adopt ST pore structure, while the other assume rather HG pore structure or stay adsorbed in the vicinity of pore rim. Such pores are therefore considered as toroidal pores (labeled as TP in above Tables.

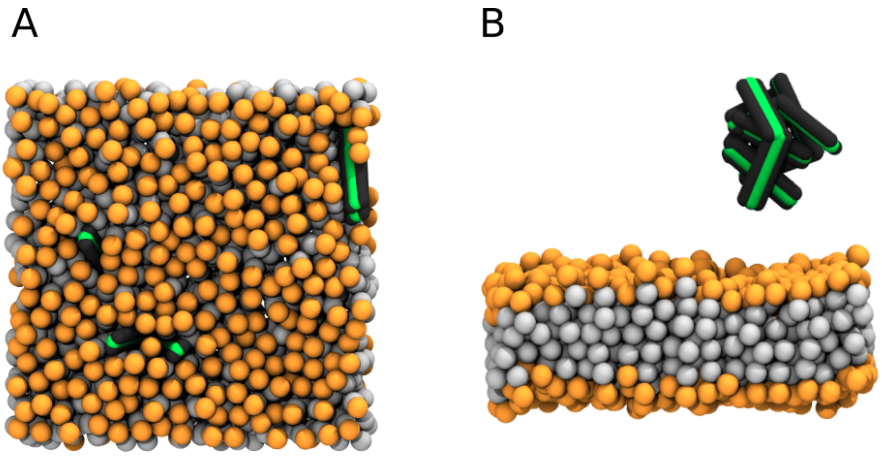

Figure S2. Example of systems with phenomenological models with disordered toroidal pore structure. (A) Rigid O-PSC-NE with 7.0 nm length and 310° *(top view)* insert into membrane independent of each other. (B) Flexible O-PSC-NE with 7.0 nm length and 310° *(side view)* form clusters in the surrounding solvent preferably. Such systems were labeled as DTP in above Tables.

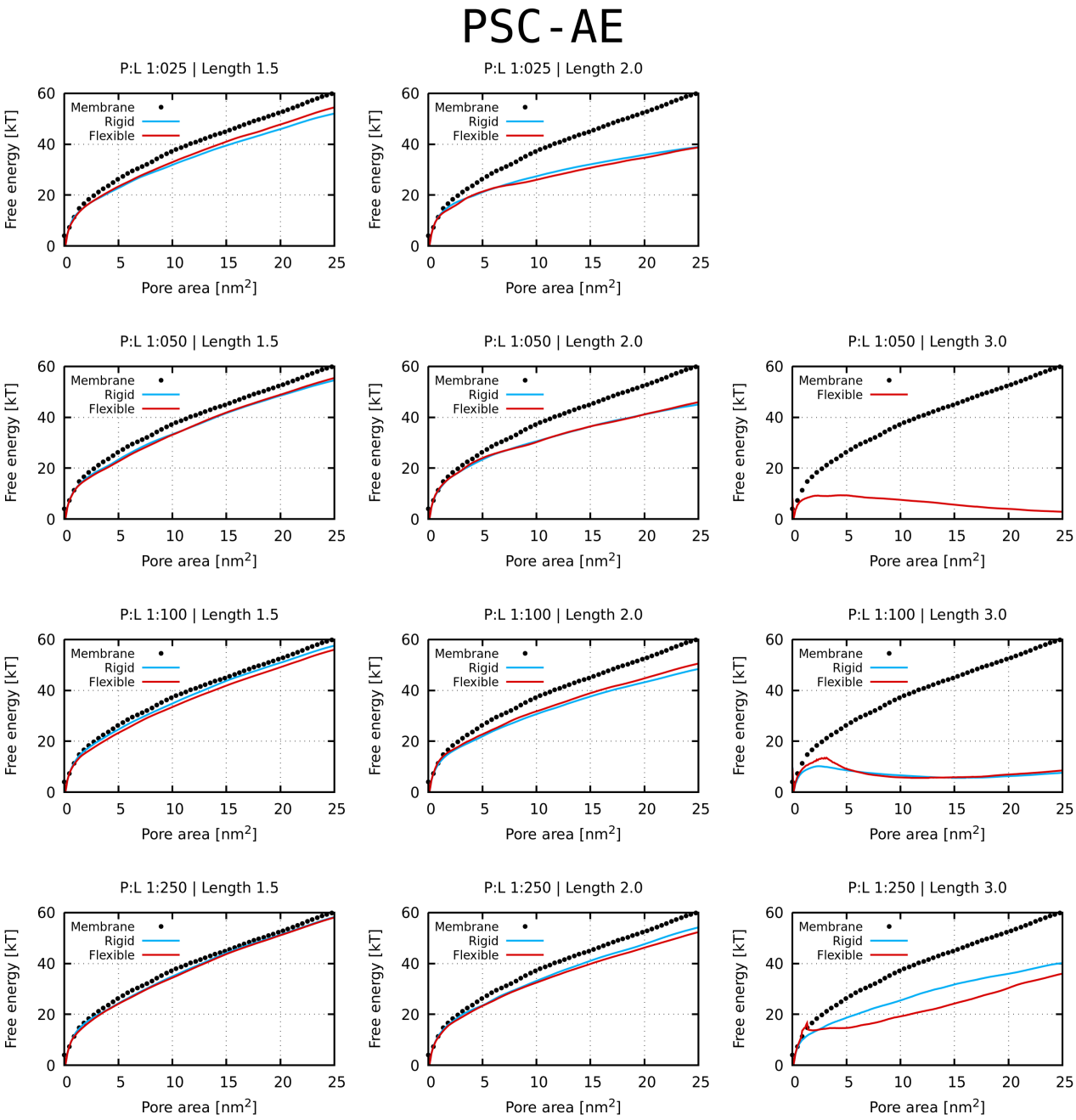

Figure S3. Free energy profiles for PSC-AE model peptides.

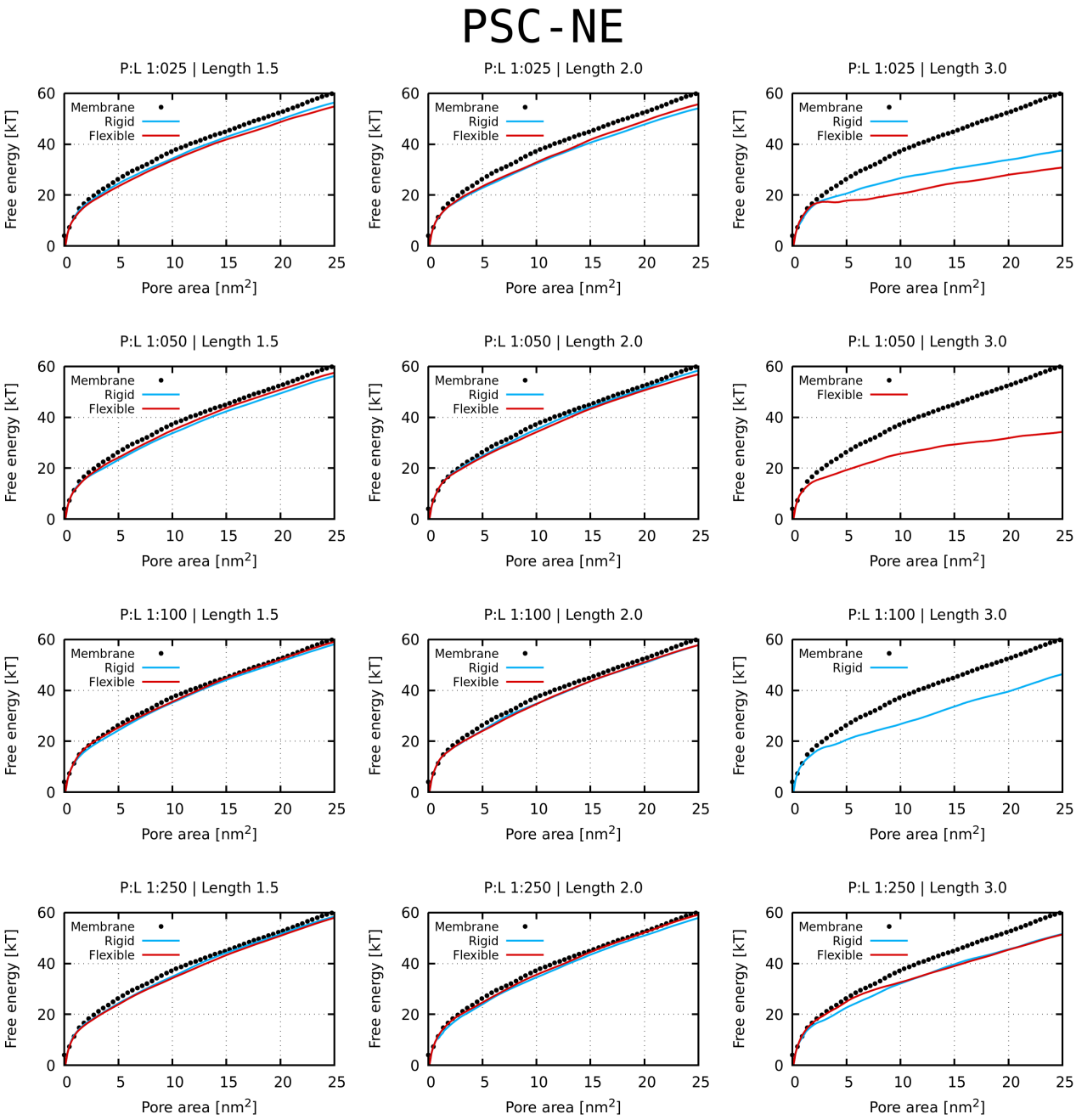

Figure S4. Free energy profiles for PSC-NE model peptides.

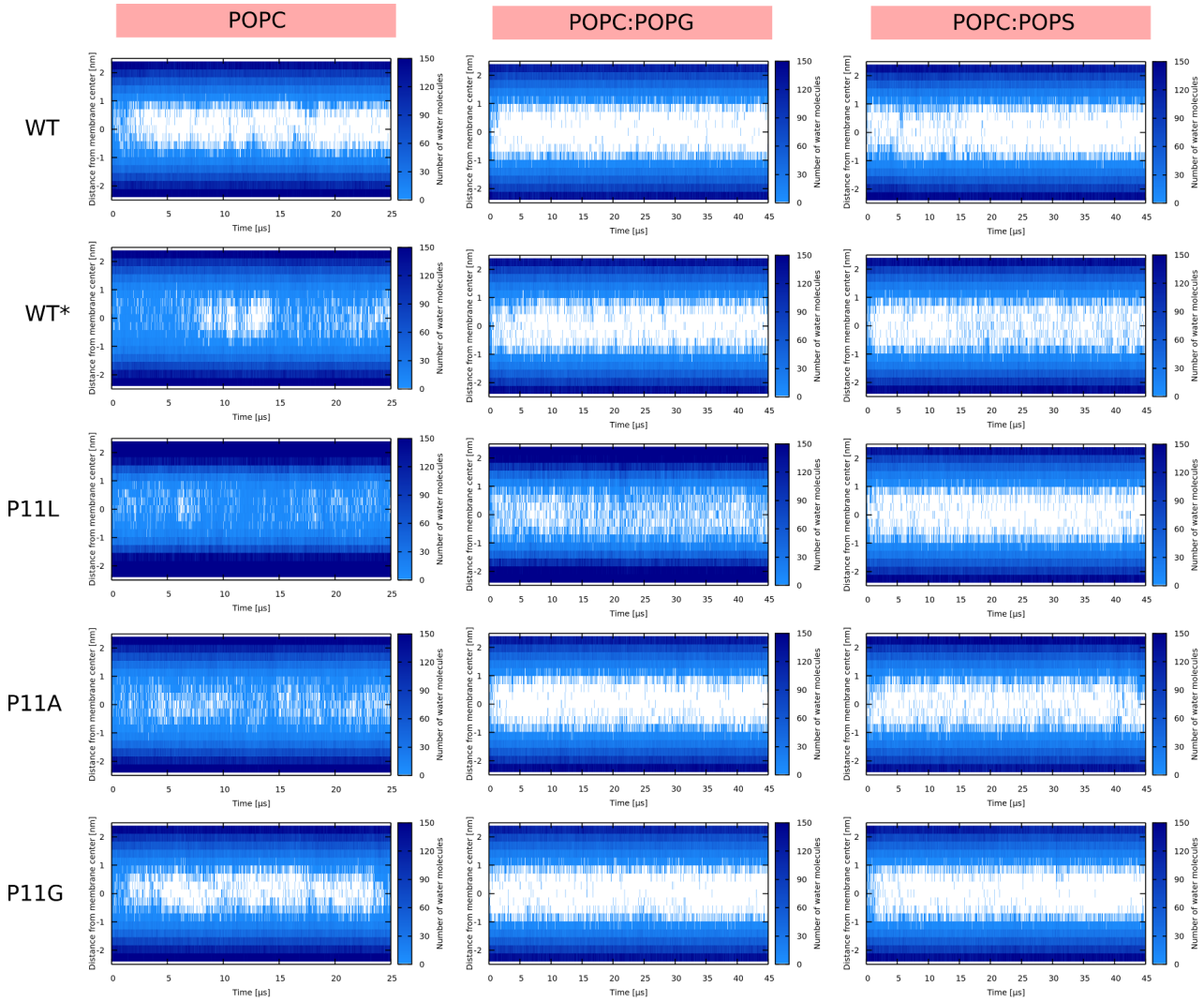

Figure S5. Water density profiles for Buforin II peptides. Note that WT$*$ stands for wild-type sequence where proline residue was forced to be α-helical.

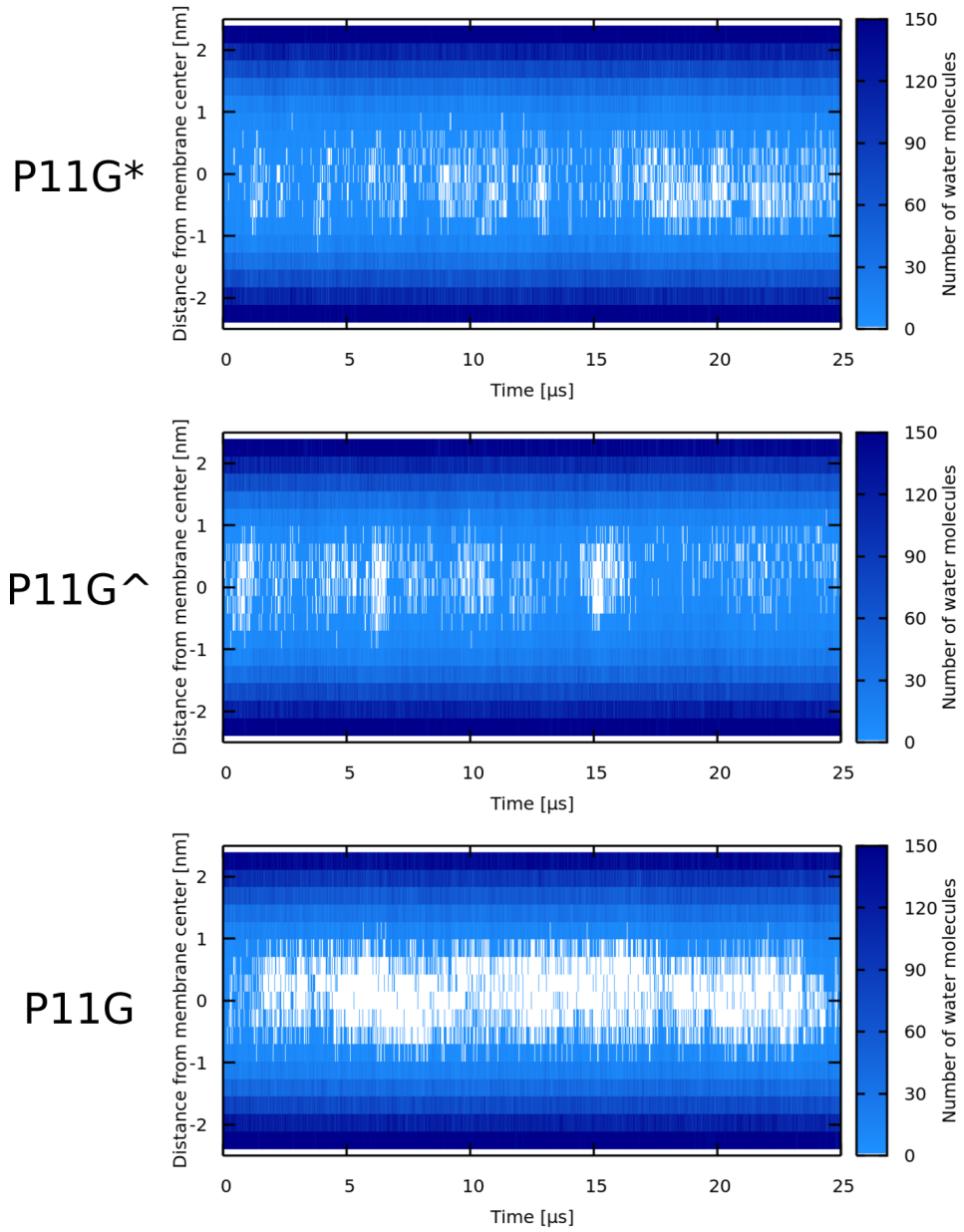

Figure S6. Water density profiles for Buforin II peptides with mutated glycine residue in POPC membrane. Note that WT$*$ stands for Buforin II P11G which was forced to be α-helical. In case of Buforin II P11G^, only single coil in mutated glycine position has been used as a definition of secondary structure.

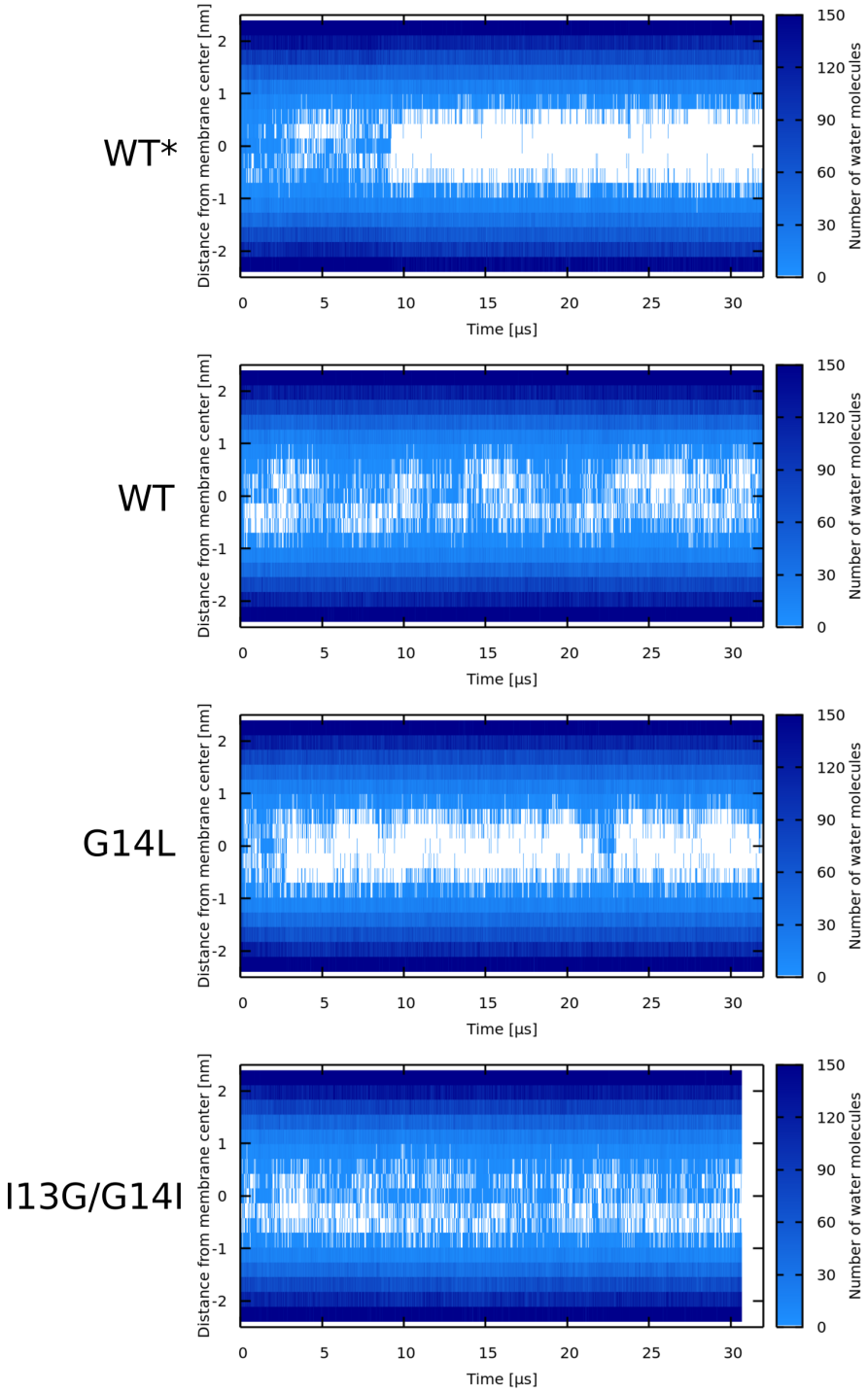

Figure S7. Water density profiles for LL-37 peptides. Note that WT$*$ stands for wild-type sequence where glycine residue was forced to be α-helical.

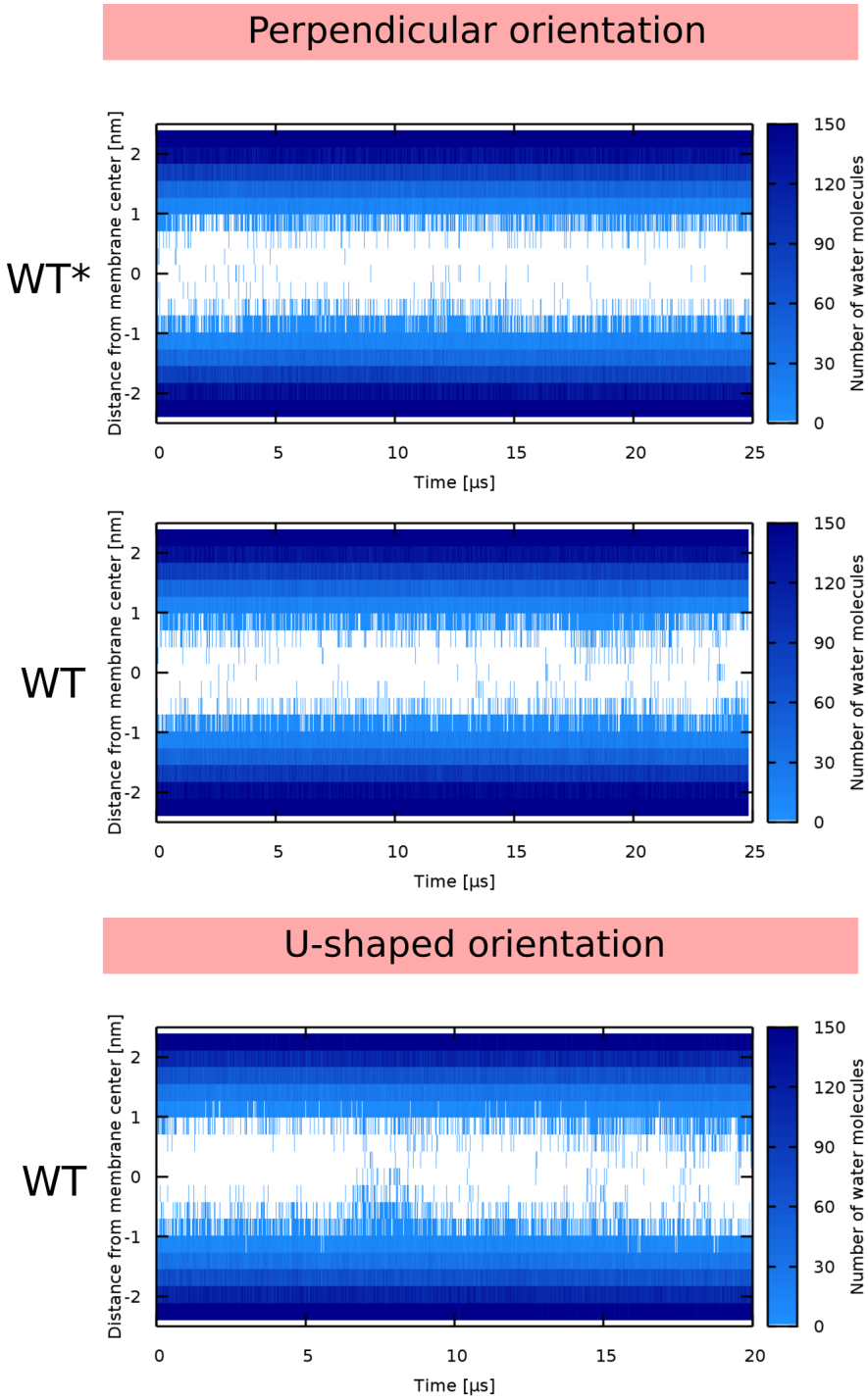

Figure S8. Water density profiles for Candidalysin peptides (CandK). Note that WT∗ stands for wild-type sequence where proline residue was forced to be α-helical.

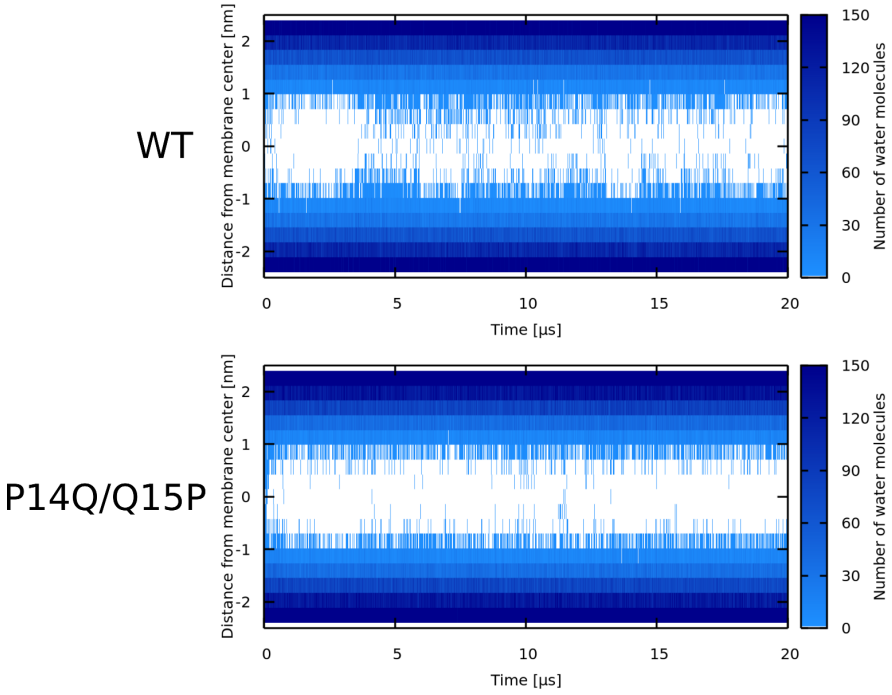

Figure S9. Water density profiles for Candidalysin peptides (CandKR). Note that WT∗ stands for wild-type sequence where proline residue was forced to be α-helical.

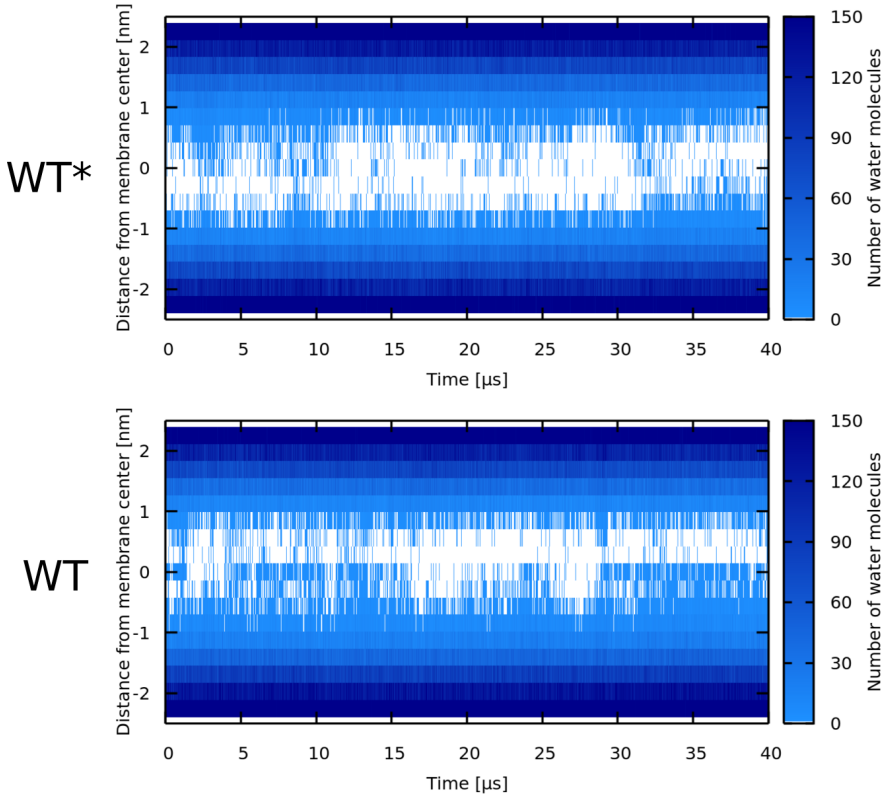

Figure S10. Water density profiles for δ-lysin peptides. Note that WT∗ stands for wild-type sequence where glycine residue was forced to be α-helical.

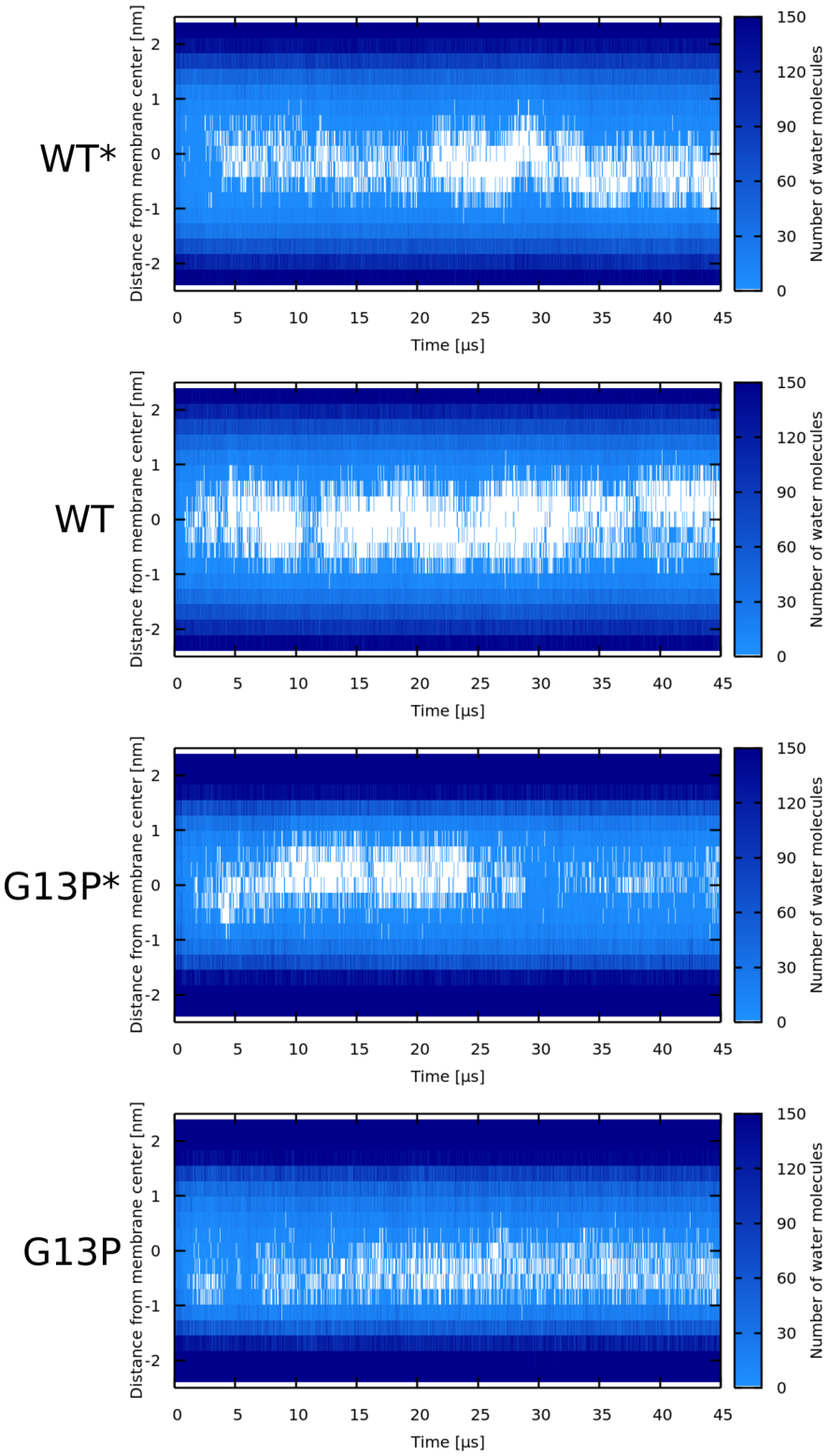

Figure S11. Water density profiles for Magainin II peptides. Note that WT∗/G13P∗ stands for wild-type sequence where glycine/mutatetd proline residue was forced to be α-helical.

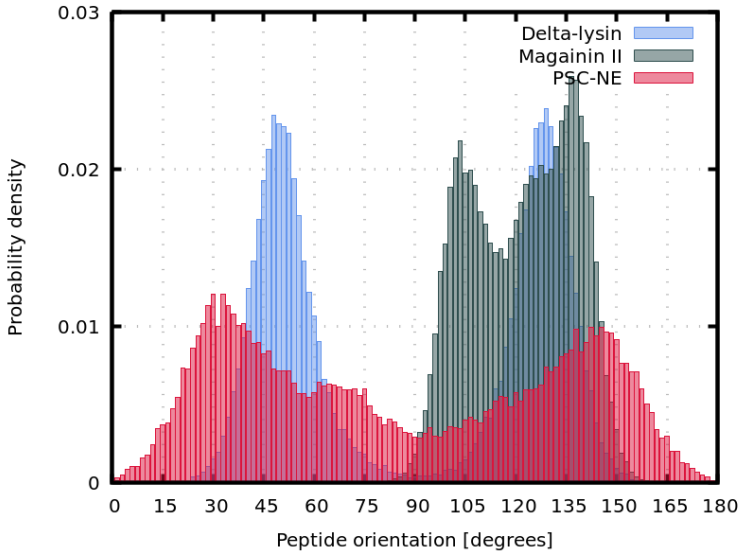

Figure S12. Comparison of angles between peptides and z-axis in systems with synergistic interactions. Phenomenological (PSC-NE) models (red), Magainin II peptides (green), and Delta-lysin peptides (blue).

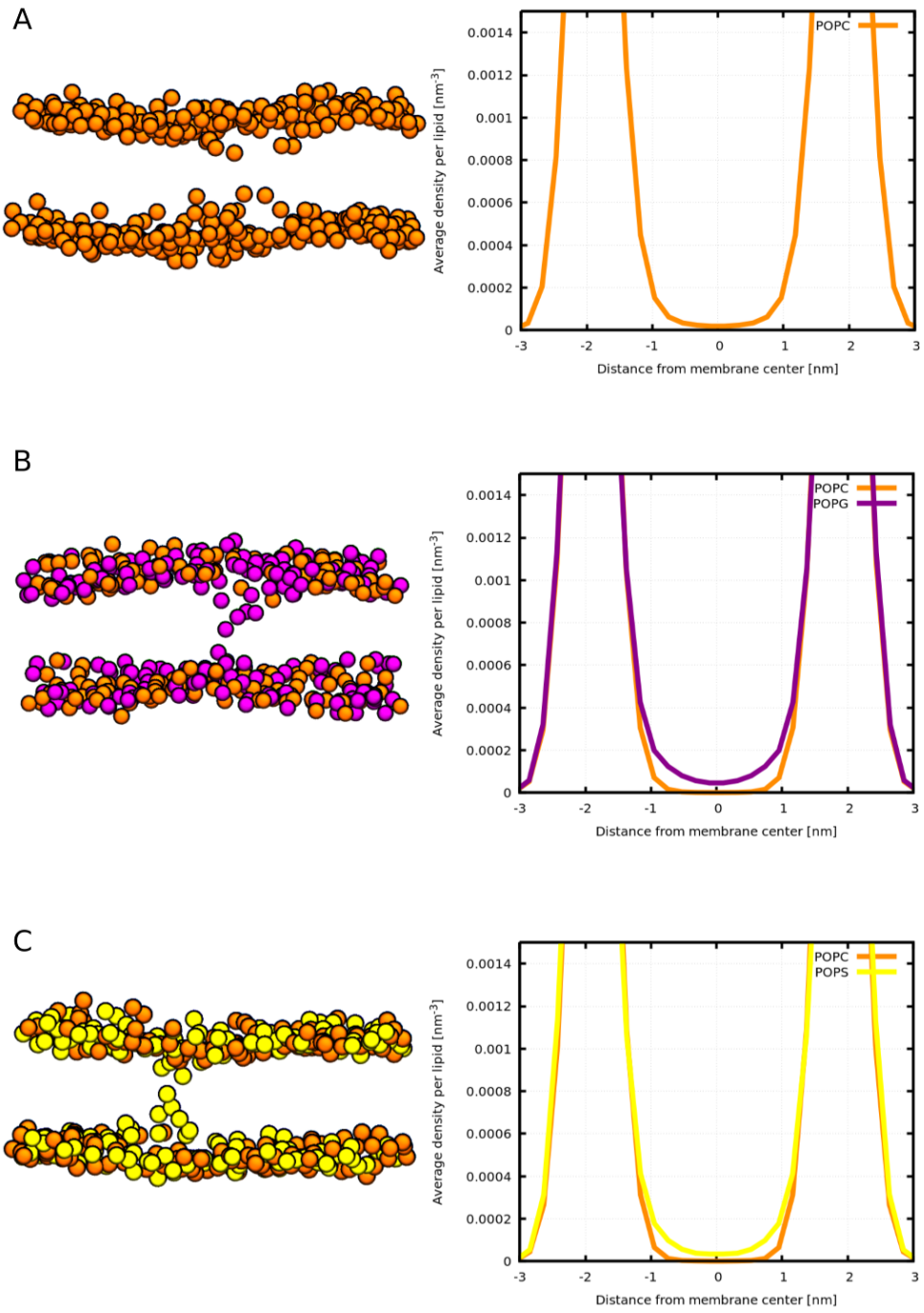

Figure S13. Density profiles and associated snapshots from Martini simulations for phosphate groups in (A) POPC membrane, (B) POPC:POPG (1:1) membrane, and (C) POPC:POPS (1:1) membrane. For a sake of clarity, only phosphate groups are depicted. Color coding: phosphate groups of POPC lipids = orange, phosphate groups of POPG lipids = purple, phosphate groups of POPS lipids = yellow.